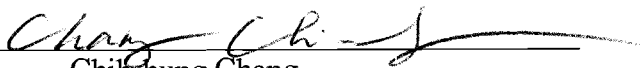AN ABSTRACT OF THE THESIS OF

Shuhong Liu for the degree of Master of Science in Chemical Engineering presented on March 4, 2005.
Title: Characterizations of Silicon-Germanium Nanocomposites Fabricated by the Marine Diatom *Nitzschia frustulum*

Abstract approved: _____

Chih-hung Chang

Marine diatoms are a class of microalgae that possess cell walls composed of silica nanoparticles. These organisms actively assimilate silicic acid $Si(OH)_4$ from seawater, polymerize silicic acid to silica nanoparticles by a protein-mediated precipitation process, and then assemble the silica nanoparticles into intricate patterns that constitute the cell wall microarchitecture (consists of around 30nm of SiO_2 nanoparticles) of the diatom frustule. The biomineralization capacity of marine diatoms, *Nitzschia,* was harnessed to biologically manufacture silicon oxide / germanium oxide nanocomposite materials. Germanium was incorporated into living diatom cell mass by a two-stage cultivation process. The micro- and nanostructures of biogenic oxide nanocomposite before and after post processing were characterized by FT-IR, HR-TEM with EDX, and XRD. Photoluminescence (PL) measurements were performed on these biogenic nanocomposites after different post processing to remove the organics. Strong blue photoluminescence was observed from samples treated with H_2O_2 and oxygen plasma. However, no photoluminescence could be observed after

800°C thermal annealing. A clear blueshift was observed from samples with the addition of germanium. Based on the comparison of the PL from diatom samples with that from synthesized silica, the self-trapped exciton (STE) affected by quantum confinement effect (QCE) is proposed as the mechanism of the PL from diatom.

Characterizations of Silicon-Germanium Nanocomposites Fabricated by the Marine
Diatom *Nitzschia frustulum*

by

Shuhong Liu

A THESIS

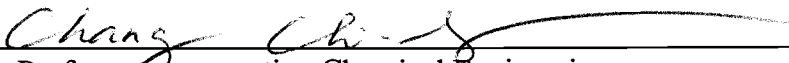submitted to

Oregon State University

In partial fulfillment of
the requirements for
degree of

Master of Science

Presented March 4, 2005
Commencement June 2005

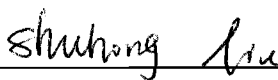Master of Science thesis of <u>Shuhong Liu</u> presented on <u>March 4, 2005</u>

APPROVED:

_____

Major Professor, representing Chemical Engineering

_____

Head of the Department of Chemical Engineering

_____

Dean of the Graduate School

I understand that my thesis will become part of the permanent collection of Oregon State University libraries. My signature below authorizes release of my thesis to any reader upon request.

_____

Shuhong Liu, Author

ACKNOWLEDGEMENTS

I sincerely express my gratitude to Dr. Chih-hung Chang, my major professor, and Dr. Gregory L. Rorrer, my minor professor, for giving me this valuable opportunity to perform this research. Not only they imparted me advanced knowledge, but also provided me financial support. Specially, Dr. Gregory. L. Rorrer's very organized attitude to scientific experiments inspired me a lot. Dr. Chang's continuous encouragement and constructive suggestions are the indispensable factors for me to finish my thesis. I would like to thank Clayton S. Jeffryes, for his up-stream work to cultivate diatom cells.

During my research, I got accessed to many facilities on OSU campus and PSU. Great thank to Dr. Christine Pastorek, the laboratory director in Chemistry Dept. at OSU, for she taught me the operation of FT-IR and gave me the permission to get access to the FT-IR facility. Thank to Dr. Jun Jiao in PSU, for she helped us to take some very useful SEM and TEM images. I would like to thank Dr. Chongmin Wang in PNNL, for his help taking some SEM and TEM images. My appreciation also is given to Dr. Jun Li in Chemistry Dept. at OSU, for her kind help for XRD analysis. I really appreciate Dr. Joa-young Jeong, he offered great help for me to get access to the system in Chem. Dept. to test the photoluminescence property so that we got the very important and precious data.

Besides, I would like to thank my fellow graduate students working in my lab for their cooperation, friendship and help. They together make a very friendly and warm working environment which is unforgettable.

TABLE OF CONTENTS

TABLE OF CONTENTS (Continued)

TABLE OF CONTENTS (Continued)

LIST OF FIGURES

LIST OF FIGURES (Continued)

LIST OF TABLES

Characterizations of Silicon-Germanium Nanocomposites Fabricated by the Marine Diatom *Nitzschia frustulum*

Chapter 1
Introduction

Marine organisms are inspirational sources of novel inorganic materials ordered at the nano and microscale[1,2]. Diatoms are living in aqueous habitats with huge amounts. They are getting more and more attention from nanotechnologists for the controlled production of nanostructured silica[3]. The advantages of diatoms in nanotechnology include:

They are made of silica which is stable container for most chemical reactions; they can fabricate three-dimensional structures, instead of layer by layer manipulation commonly found in present nanotechnology; diatoms can produce nano-silica particles continuously via exponential growth of their numbers.

Nanostructured silicon-germanium composite materials exhibit novel optoelectronic properties which can be used for photodetector and photovoltaic applications[4]. Current methods for the fabrication of nanostructured Si-Ge composite materials usually require high temperature, near vacuum conditions and expensive equipment. Since germanium is in the same group as silicon in the Periodic Table of the Elements, diatoms might convert germanium to be nanostructured germanium oxide following the similar mechanism with the formation of nano-silica. This is the rationale of this project.

A two-stage cultivation process allows the photosynthetic marine diatom *Nitzschia frustulum* to assimilate soluble germanium and fabricate Si-Ge oxide nanostructured composite materials is reported in the MS thesis by Clayton S. Jeffryes[5]. The characterization of the material cultivated by a two-stage cultivation process is accomplished in this thesis. Various techniques, such as FT-IR, XRD, TEM, SEM-EDS and Photoluminecence spectrometer, were used to characterize the material and the results are reported in this thesis.

Chapter 2
Literature Review

2.1 Nanotechnology

Ever since physicist and Nobel laureate Richard Feynman's seminar entitled "There's plenty of room at the bottom" in 1959 [6], which predicted that nanotechnologists would be able to build complex machines and circuits atom by atom, researchers have started the revolution of nanotechnology. Nanotechnology concerns materials and systems whose structures and components exhibit novel physical, chemical and biological properties, phenomena and processes due to their nanoscale size[7]. Nanotechnology aims at controlling properties at nano-scale level and realizing components with dimensions below 100nm. The development of nanotechnology is closely related to the discovery of novel nanomaterials, which typically contain building blocks, nanoparticles, structurally feature on the scale of 1 to 100 nm. The nano-scale endows nanomaterials with many unique properties such as optical, magnetic, dielectric or mechanical properties. Therefore, nanotechnology provides spectacular potential applications in various aspects[8].

(i) Medicare

Nanotechnology is finding promising applications in medicare, such as drug delivery capsules, in-vitro sensors, membranes for chemical purification and nanorobots. For example, diseases are caused largely by damage at molecular and cellular level, but today's surgical tools are too large to deal with molecules and cells. The dream is to build medical nanorobots smaller than a cell and then solve the problem. They could roam human bodies eliminating bacteria and clearing out

clogged arteries. Nano-sensors could detect cancer tumors at their early stage, so the patients could receive effective early treatments.

(ii) Transportation

As business and human activities become more global, the demand for higher quality and more reliable operation of transportation systems increases considerably. The big challenges in transportation are to improve the robustness of transportation systems for decreasing or eliminating air pollution; to create lighter and stronger materials for constructing safer aircraft and vehicles, and to create more effective detectors for monitoring drugs and other chemicals for security purposes. Nanotechnology will make great impact on transportation in the coming future both in civilian and military applications, to list a few examples:

(a) Stronger and lighter materials with nanoscale dimensions that lead to faster, cheaper, and safer transportations.

(b) Nano-catalysts that can reduce or eliminate the emission of pollutants from engines that is released to the environment.

(c) Photonic nanodevices to replace the heavy and costly RF transmission equipment on aircraft, ships, or satellites.

(d) Highly sensitive nano-scale chemical sensors for detecting trace chemicals

(iii) Electronics

The fabrication of modern semiconductor electronics systems, such as computers and wireless communication systems greatly depend on nanotechnology. Microprocessor designer, Nick Tredennick, helped design the Motorola 68000CPU,

believes that nanotechnology has the potential of leading the semiconductor industry to long-term growth and eliminating the boom-and-dust cycles. One of the most important techniques to fabricate nanoelectronics is photolithography. As the chip components continue to shrink toward the nanoscale and silicon devices become more and more complex, creating the masks to make nano-features via photolithography will be a big challenge and becomes prohibitively expensive. In order to solve this problem, researchers are looking forward to a "maskless" process in which circuitry patterns as small as 10 nanometers are made without photolithography, but through molecular self-assembly.

"Moore's Law" is well-known in electronic field[9], which predicts the number of transistors per square inch on integrated circuits doubles approximately every 18 months. This implies smaller and smaller feature sizes. For more than a decade, researchers have followed the pace of Moore's Law by introducing new generation processes approximately every 18 months. Now the most advanced nanoelectronics have been realized is the 90nm technology developed by Intel Corp., which puts this technology into volume manufacturing exclusively on 300-mm wafers. This combination allows Intel to make better products with reduced manufacturing costs. Along this path, 65 nm products are expected to be the next generation of nanoelectronics. The modern complex and portable electronic products would not be realized without the development of nanotechnology.

Nanotechnology has tremendous potentials that will considerably improve human's life in the near future, so it has not only attracted numerous researchers' but

also political leaders' attention. The former President of the United States (William Clinton, Jan. 21, 2000) had called for a $500 million National Nanotecdhnology Initiative and encouraged people to imagine " materials with ten times the strength of steel and only a small fraction of the weight…shrinking all information housed at the Library of Congress into a device the size of a sugar cube…detecting cancer tumors when they are only a few cells in size." Also the current President of the United States signed the "21st Century Nanotechnology Research and Development Act" in December, 2003. This legislation placed the programs and activities supported by the National Nanotechnology Initiative (NNI) as one of the President's highest multi-agency R&D priorities.

Despite the technological and economic promise of the devices, the fabrications of the current commercial nano-products exist a number of challenges, such as strict synthesis conditions, harsh working environment, laborious workloads and limited resources etc. Particularly, most methods in commercial nanoelectronics were based on planar lithographic approaches (2 dimensional) developed for microelectronics industry[10], for instance, silicon micromachining by photolithography and chemical or plasma etching. On the other hand, 3 dimensional nano-devices with complicated geometries and features will impose significant challenges on the common planar approach for mass production of 3 dimensional nano-devices at low cost.

2.2 Diatom biomineralization

Diatoms are microscopic single celled plants that inhabit both marine and fresh water environments. They are more than 10^5 species[11], and each of them forms unique

frustules (cell walls) made of nanoporous networks of amorphous silica composites. Usually, diatoms are classified into two groups according to their frustules' shape, pennate and centric. Pennate diatom frustules are featured with bilateral symmetry and an elongate pattern center and contain mostly parallel rows of pores perpendicular to the long axis, whereas the centric species exhibit radially symmetrical pattern with pores extending radially from the center to the circumference. Diatoms play a important role in nature in producing oxygen and as the basis of the aquatic food chain.

In the past, diatoms have been studied as model organisms to investigate the biochemical basis of biogenic silica formation. Recently, they got more attention from nanotechnologists, because their intricate microscopic glass structures of cell walls may also be a valuable resource for nanotechnology. They could act as tiny moulds to fashioning lenses for optical computers and growing gears for micro-robots. "The advantage with a diatom is that it grows complex structures in three dimensions directly," says Richard Gordon, a diatomist at the University of Manitoba, Canada. "Most human technology can only do 3D by building layer after layer and so far none can match the diatom for complexity."[12]

Marine organisms have long been an inspirational source for novel nanomaterials, because they incorporate inorganic elements such as calcium and silicon into their structures, such cell walls, with both nanometer and micrometer structures. Meanwhile, they have the ability to make complex nanoscaled three-dimensional structures at ambient conditions and in large number. These advantages are superior for silica fabrication compared with current manufacture techniques in industry, which usually

are two dimensional and rely on high temperature. The incorporating process of inorganic elements in diatoms is generally called biomineralization. The silicon metabolism in diatoms was reviewed by Martin-Jézéquel et al[13]. Silica transporter (SIT) proteins imbedded in the cell wall of the organism bring soluble $Si(OH)_4$ (silicic acid) into the cell[14]. The biomineralization process of silica takes place within the silica deposition vesicle (SDV). The SDV is formed in the interior of the plasmalemma following cytokinesis[15]. Additional work revealed that silicic acid uptake was tightly coupled to cell wall silicification and an apparent feedback mechanism controlled the uptake according to the demand for silica deposition[16]. The major component that catalyzes the condensation and precipitation of silicic acid to hard monodisperse silica nanospheres is called silaffin (a polypeptide). The silicon uptake process utilizing silica transporter proteins and the process of silica precipitation to hard silica nanospheres controlled by silaffin proteins are illustrated in Fig.1[17]. As the cell divides, the newly formed silica nanoparticles form the new epitheca of the daughter cell.
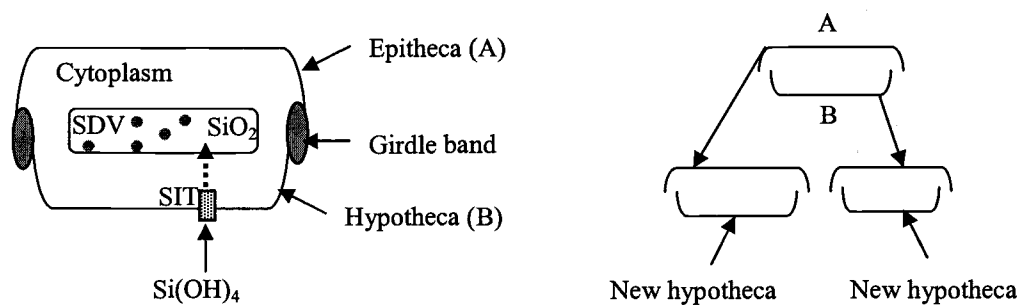
Fig.1 The illustration of biomineralization process of silica and division of diatom cell

The silaffin1A_1 has been isolated from the shell of the diatom *Cylindrotheca fusiformis* by Nils Kröger and his team in 1999[3], and the silaffin 1A_2 has been separated from the same species of diatom by the same group in 2002[16]. The structures of silaffin1A_1 and 1A_2 are shown in Fig.2. Their silica-precipitating activity depends on the presence of modified lysine residues. Silica particles with diameter of 500-700nm have been precipitated with the catalysis of silaffin 1A, and diameter of less than 50nm with the mixture of silaffin *in vitro*. The size distribution of silica particles precipitated utilizing silaffins *in vitro* is not as uniform as that synthesized *in vivo*.

Silaffin 1A_1

NH₂—S—S—K—K—S—G—S—Y—S—G—Y—S—T—K—K—S—G—S—CO₂H
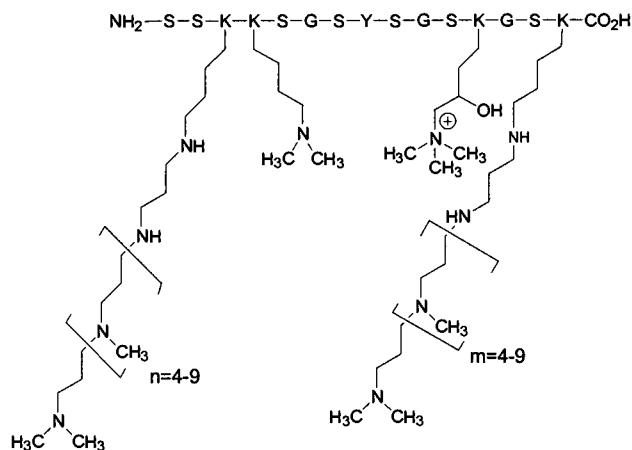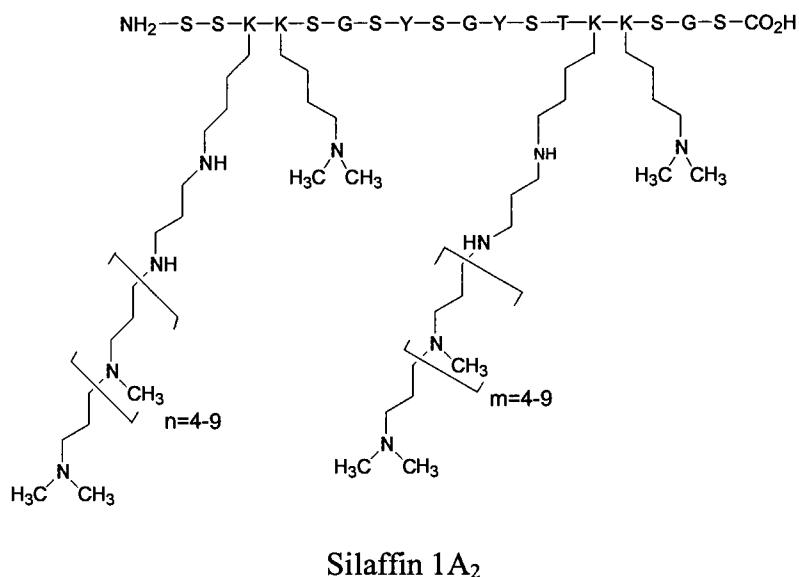
Silaffin 1A₂

Fig.2 Chemical structures of silaffin1A₁ and 1A₂

The nanospheres of silica range from 3 to 50 nm depending on the species[18], but nanosphere diameters within a given diatom cell frustule are often monodisperse[19,20]. The microscale patterns created by nanosphere deposition are also species specific and are replicated upon cell division, suggesting molecular genetic control of the assembly process[12].

To a nanotechnologist, diatoms seem to be a very promising nanomaterial fabricator. Because they not only made precision, three-dimensional structures quickly, cheaply and in numerous quantities, but also fabricated materials at room temperature and atmospheric pressure, without the usage of toxic chemicas.

Scientists are currently exploring different approaches to fabricate nano-materials and nano-devices by diatoms. Some of them are using diatom shells with a particular pore size as reaction vessels. For example, Thomas Manning used the shells of the diatoms, *Arachnoidiscus* and *Actinocyclus*, as "ice cube trays" for growing manganese

acetate (Mn12) nanocrystals[10]. Although Manning's team has not been able to make Mn12 crystals because the diatoms they used have overly large pores, they believe that the technique has a great potential for making nanocrystals of other compounds. Other scientists are looking for ways to convert the glassy shells into other desired materials while preserving their structures, or to harness their glass-mould proteins to grow devices without diatoms themselves. Mary Ann Tiffany has found that diatoms create an array of intermediate structures which looks like gears as their shells mature. They proposed to break these "gears" off and put a shaft through the middle. Apparently, glass is not an ideal material for gears or other mechanical components, so a process to change diatom shells atom by atom from glass into other substances has been invented by ceramic chemist Ken Sandhage[21]. This process is to bake shells of the diatom *Aulacoseira* at 900 °C in the atmosphere of magnesium gas, transforming silica into magnesium oxide while preserving their structure.

Since diatoms have the great ability to fabricate nanostructured-silica materials, the idea of making other nano-metal oxide is attractive. Fabricating nanostructrued germanium-silicon composite is a particular interest, because it exhibits novel semi-conducting and optoelectronic properties for microelectronic and optoelectronic applications. Germanium is a group IV semiconductor just below silicon in the Periodic Table of Elements. It is well known that soluble germanium inhibits cell division in diatoms. However, it is not known if diatoms can assimilate germanium into their silica nanostructure. Previous work using [68]Ge radioisotope labeling has showed that heterotrophic marine diatom *Nitzschia alba* rapidly assimilated soluble

germanium[22,23]. A later TEM study showed that concentrations of 0.07 mM $Ge(OH)_4$ and 0.7 mM $Si(OH)_4$ in the culture medium (10:1 ratio of Si to Ge) induced aberrations in *N. alba* frustule morphology[24].

Current technology for the fabrication of nanostructured Si-Ge semiconductor composite materials usually involves fairly exotic processes operating at high temperature and near vacuum conditions. Does the emerging field of "diatom technology" offers an alternative route to these materials? Our working hypothesis is that the nanobiochemical machinery of the diatom cell can be harnessed to fabricate nanostructured germanium and silicon oxide materials using a simple, room-temperature bioprocessing platform. The objective of this study was to characterize the nanostructrue and observe the optical property of the Si-Ge nanocomposite fabricated by marine diatoms.

Chapter 3
Materials and Methods

The overall flowchart of the diatom culture cultivation process and characterization process of the post-cultivation is illustrated as Fig.3.

```
                        ┌─────────────────────┐
                        │  Culture Cultivation │
                        └─────────────────────┘
                                  │ (Cell Mass)
                                  ▼
                        ┌─────────────┐      ┌─────────┐
                        │  Air Drying  │─────▶│   ICP   │
                        └─────────────┘      └─────────┘
                                  │
          ┌───────────────────────┼───────────────────────┐
          ▼                       ▼                       ▼
   ┌──────────────┐      ┌──────────────────┐    ┌──────────────────┐
   │ H₂O₂ treatment│      │ O₂ plasma etching│    │ Annealing(800°C) │
   └──────────────┘      └──────────────────┘    └──────────────────┘
```

H_2O_2 treatment O_2 plasma etching   Annealing(800°C)

Photoluminescence   TEM/EDS   SEM   FT-IR   XRD
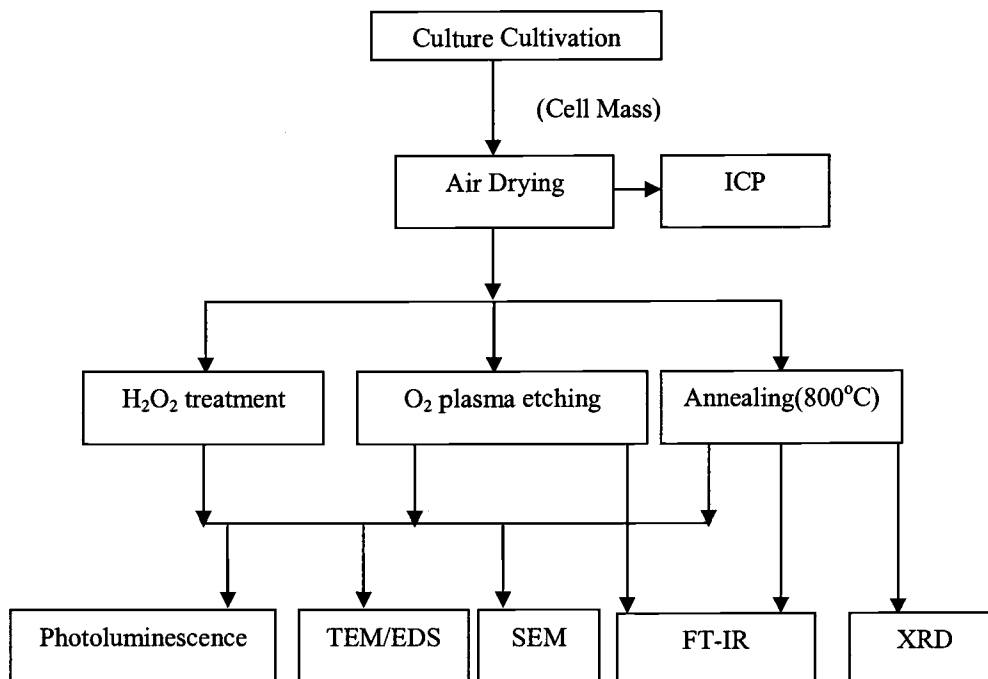
Fig.3 Flowchart of the cultivation and characterization process

The work of the cultivation of the diatom culture was not conducted in this thesis (the cultivation process was reported by Clayton Jeffryes[5]),

3.1 ICP-AES

Inductively coupled plasma-atomic emission spectrometry (ICP-AES) is one of the most common techniques for elemental analysis. The analysis is usually performed by preparing a sample solution that is transformed into an aerosol by means of a nebulizer. The small droplets in the aerosol are transported through a spray chamber towards a

high temperature Ar-plasma. The plasma effectively excites the material in the sample at a temperature of about 7000 K. This results in free atoms and ions in a higher energy level, which energy will lose by emitting light when the excited atoms or ions return to their ground state. The intensity of the light is proportional with the concentration of the specific element. This element-specific radiation is highly characteristic and can be measured by a spectrometer.

The purpose of ICP-AES analysis here is to study what major inorganic elements are contained in the diatom cell and to measure their relative content. The sample preparation procedure is as follows: Add 50 mg of ground cell mass (without etching or annealing) that has been weighed to the nearest 1 mg to a Ni crucible containing 0.5 g of solid ground NaOH. Cover the crucible and heat it to 400 °C for 15 min. After the fusion is cooled, add 50 ml of DI water. 1 hour later, transfer the dissolved fusion to a plastic beaker and acidify it with 2 ml of 93% H_2SO_4. Up to this point, the solution is completely clear. Then take about 20 ml of the clear solution to run ICP analysis.

3.2 Thermal annealing

The purpose of thermal annealing is to remove the organic materials contained in diatom cells, so that it will be easier to observe skeleton shape and measure the composition of the inorganic material left over. The diatom cell mass was washed with 100 mM NaCl, and then dried in air at room temperature. The air-dried cell mass, composed of a coarse green powder, was evenly spread out within a nickel crucible and heated in a furnace for 7 hrs at 800 °C in still air. During thermal annealing in air, carbonaceous material in the cell mass was oxidized to CO_2, yielding a fine, residual

white powder enriched in the biogenic inorganic material. After annealing, the sample mass was lost about 50%. Thermally annealed samples were stored in a desiccating chamber at room temperature.

3.3 Oxygen plasma ashing

Oxygen plasma ashing was also carried out for the same purpose as thermal annealing, and it also served as a comparison of the characterization result with thermal annealing. The diatom cell mass was washed with 100 mM NaCl, then dried in air at room temperature. The air-dried cell mass composed of a coarse green powder, was evenly spread out within an aluminum container and placed in an oxygen plasma asher for 1 hour, with RF power 400W. During ashing, carbonaceous material in the cell mass oxidized to CO_2, yielding a fine, residual white powder enriched in the biogenic inorganic material. After ashing, the mass loss was about 50%. Ashed samples were stored in a dessicating chamber at room temperature.

The schematic diagram of oxygen plasma asher is illustrated in Fig.5. When an electric potential is applied to O_2 gas at a reduced pressure (1mtorr-1torr), some O_2 molecules could be dissociated and electrons are generated. Those electrons could get more energy and collide with other molecules, so more and more molecules are dissociated. Compared with elastic collision, inelastic collision is a very efficient way to disperse energy, such as excitation, relaxation and ionization. The excited electrons remain in a bound state and will radioactively decay, giving off light that is the reason why the plasma glows. The plasma is sustained by the inelastic ionization process. One of the attractive advantages of using plasma to remove materials is that the

temperature is always lower than 100 °C , which can avoid many side reactions. The overall reaction taking place in plasma chamber is as follows.

$$e^- + O_2 \rightarrow 2O^* + e^- \tag{1}$$

$$2O^* + C \rightarrow CO_2 \tag{2}$$

O^* represents oxygen radical, which is very reactive.
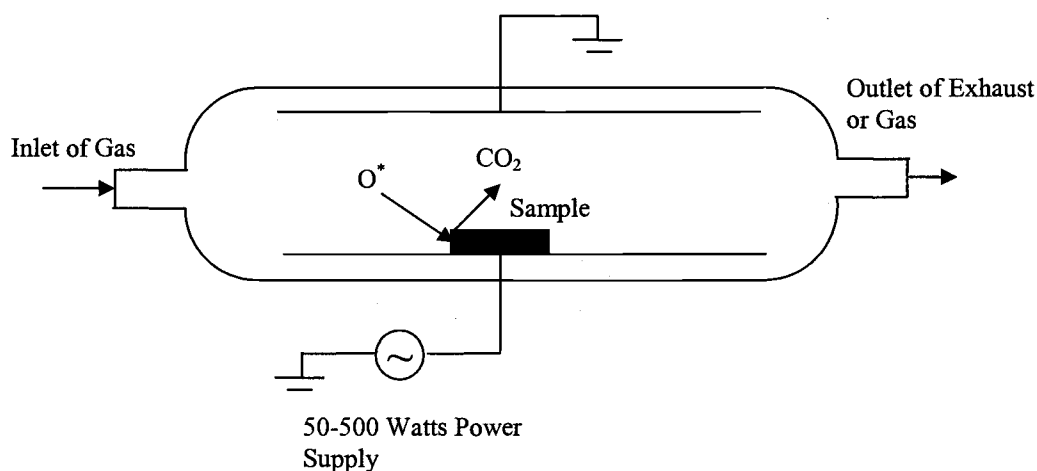
Fig.4 Schematic diagram of the oxygen plasma barrel asher

3.4 SEM-EDS

Scanning electron microscopy (SEM) is used for inspecting topographies of specimens at high magnification. During SEM inspection, an electron beam is focused on the specimen, resulting in the transfer of energy to the spot. These bombarding electrons, also referred as primary electrons, dislodge electrons from the specimen itself. The dislodged electrons, also known as secondary electrons, are

attracted and collected by a positively biased detector, converted to a voltage, and amplified, then translated into a signal.

To produce a SEM image, an electron beam is swept across the area being inspected, producing many such signals. These signals are then amplified, analyzed, and translated into images of the topography being inspected. When the electron beam is projected on a spot, if a large number of secondary electrons are detected, a bright spot on the surface of Cathode Ray Tube (CRT) monitor will be resulted. If the electron beam moves to a depression on the sample, fewer electrons will be detected and a smaller voltage will be detected in the detector, resulting in a darker spot on the surface of the CRT. Finally, the SEM image consists of spots with varying intensity on the face of a CRT, corresponding to the topography of the sample.

The purposes of SEM measurements are to observe the surface topography of the diatom frustule, measure the size of the pores on the surface of the skeleton. Three SEM sample preparation methods were tested, including thermal annealing, oxygen plasma ashing and chemical treatment using hydrogen peroxide. The method using hydrogen peroxide is described in the MS thesis of Clayton Jeffryes[5].

Prior to putting sample into the SEM chamber, sample was dispersed and sputter-coated with carbon. Scanning electron microscopy relies on the ability of a compound to interact with an electrical current, so its resolution is limited to the surface conductivity. Otherwise, the electrons will be built up on the sample surface. SEM images of the cleaned *N. frustulum* frustules were obtained at Oregon State University using an AmRay 3300 field emission scanning electron microscope (FESEM).

Some SEM images were obtained from the microscopy facility at Portland State University. Carbon tape was affixed to aluminum stubs and the respective sample powders were dispersed onto the carbon tapes. A FEI Sirion FESEM (ISI), 30keV microscope was used to image the samples at accelerating voltages of 5.00 KeV and 2.00 KeV and at a working distance of 5 mm. An SS40 SEM (ISI), 30keV microscope, equipped with an Oxford ISIS EDS system was used to do EDS on the samples.

Energy Dispersive Spectroscopy (EDS) is a standard procedure for identifying and quantifying elemental composition of sample areas as small as a few cubic micrometers. The characteristic X-rays are produced when a material is bombarded with electrons in an electron beam instrument, such as a scanning electron microscope (SEM). Detection of these x-rays can be accomplished by an energy dispersive spectrometer, which is a solid state device that discriminates among X-ray energies.

3.5 TEM-EDS

Transmission Electron Microscopy (TEM) is a technique used for analyzing the microstructure, crystallographic structure, and composition of a specimen. TEM provides a much higher spatial resolution than SEM, and can facilitate the analysis of features at atomic scale (in the range of a few nanometers) using high energy electron beam typically in the range of 60 to 400 keV.

Unlike SEM, which relies on dislodged or reflected electrons from the specimen to form an image, TEM collects electrons that are transmitted through the specimen. Also the specimen for TEM analysis should be very thin, so that electrons can penetrate through. Electron beam is produced by electron gun and then controlled to

strike the specimen. This beam gets transmitted to the other side of the specimen, is collected, and recombines to form the image appeared on the phosphorous screen.

The purposes of the TEM analysis are to observe internal structure and to analyze the elemental composition of the diatom skeleton. The thermally annealed and plasma etched diatom cell mass, consisting of a white powder, was ground in mortar and pestle to break apart the microscopic diatom shells. This ground powder was then re-suspended in acetone and pipetted onto a copper TEM grid coated with a Lacey carbon film. These samples were observed by transmission electron microscopy (TEM) at 200 KeV using a Tecnai F20 field emission TEM equipped with an embedded scanning transmission electron microscope (STEM) and energy-dispersive x-ray spectrophotometer (EDS) at Portland State University, Portland, Oregon. (Some samples were also observed at 60KeV using a Pholips CM12 TEM at Oregon State University.) Once a representative nanocluster was identified by TEM, EDS analysis in line-scanning mode was performed (200 KeV, 15 nm increment, 5000 msec per increment).

3.6 TEM sample sectioning (ultramicrotomy)

Besides the annealed and plasma etched powder samples, some sectioned very thin slice specimens were also prepared for TEM analysis. The major purpose of sample sectioning is to study the location of germanium. There are two reasons for improved resolution with thinner specimens. First of all, the electron beam of the accelerating voltage used in most TEMs has limited penetration capabilities. Second, the depth of field of the objective lens in the TEM leads to the superimposition of the detail of the

specimen in the micrograph, making individual features hard to see with conventional micrographic means.

The sample sectioning process is described as follows. Put a little etched (or annealed) powder sample into a suitable mold (a small plastic tube), then add a volume of fresh SPURR's resin to embed the specimen. Vacuum the mold several times to remove the air in the sample and resin. Otherwise the air bubble will make the sectioning process uneven, therefore affect the quality of the final slices. Put the mold into oven and heat it at 50 °C for 24-48 hours to polymerize the resin.

After the specimen has been casted into a block of resin, trim the specimen block down to a level where the specimen is exposed at the surface. This step was done by holding the block in a microtome chuck under a low magnification and carving the resin away with a razor blade. The specimen face was trimmed up into a truncated pyramid with a face of trapezoid. The block was then mounted in another microtome, and a few sections about 100 nm thick were cut. The ultrathin sections were removed from the boat and dried onto a glass slide for TEM.

3.7 FT-IR

Fourier Transform Infrared (FT-IR) spectroscopy is a very common technique to obtain the bond information of chemical substances. When radiation passes through a sample, certain frequencies of the radiation are absorbed by the molecules of the substance leading to the molecular vibrations. The frequencies of absorbed radiation provide the characteristics of a substance. FT-IR spectrum is obtained by first collecting an interferogram of a sample signal using an interferometer, and then

performing a Fourier Transform on the interferogram to obtain the spectrum. Unlike dispersive spectrometer (grating monochromator), in which wavenumbers are observed sequentially as the grating is scanned, FT-IR spectrometer collects all wavelengths simultaneously. This makes the signal collection much faster (1s) than using dispersive spectrometer (30min).

A Nicolet 510P FT-IR spectrophotometer equipped with DTGS detector (4 cm^{-1} resolution) was used to obtain FT-IR spectra of the thermally annealed, etched and original cell mass. An aliquot of the sample (typically 2 mg) was ground in 100 mg KBr to a fine powder, and 40 mg of this mixture was loaded into the FT-IR cell. FT-IR analyses were performed in transmission mode. FT-IR measurements were conducted in the Chemistry Department at OSU.

3.8 XRD

X-ray diffraction (XRD) is a technique to measure the plane distance (d) of periodically ordered substance, such as crystal or powder crystalline grains. The short wavelengths of X-rays (a few of angstroms) are comparable to the size of atoms, so they are ideally suited for probing the structural arrangement of atoms and molecules. The incident X-rays interact with atoms of the sample. If the atoms or molecules arranged periodically, and the Bragg's law (shown in equation 5) is satisfied, the X-ray diffraction occurs.

$$2d \cdot \sin\theta = n \cdot \lambda \tag{3}$$

Where d: inter-plane distance of the substance;

θ :X-ray scattering angle;

n: an integer representing the order of the diffraction peak;

λ: X-ray wavelength.

Based on equation (5), the inter-plane distance d can be calculated for a specific order of diffraction peak. Therefore the peaks in an X-ray diffraction pattern are directly related to the crystal structure. The crystal structure for each substance is unique, so X-ray diffraction can be used to identify the materials.

The XRD spectrum of the thermally annealed cell mass was obtained using a Siemens D5000 X-ray diffractometer with a CuK radiation source at 2θ resolution of 0.02°. Typically, 0.1g thermally annealed powder was ground to fine powder. The sample holder surface was coated with a thin layer of glycol. The powder was evenly dispersed on the surface of the holder, and the holder was placed into the diffractometer. XRD measurements were carried out in the Chemistry Department at OSU.

3.9 Photoluminescence

PL measurements were performed at room temperature using the instrument in the Chemistry Dept. at OSU. The powder sample was sticked on the surface of a square blackboard (2cm × 2cm) by grease. The blackboard with powder sample was inserted inside a holder that was oriented to the light beam by 45°.

The PL measurement system is illustrated in Fig.6. All instruments were manufactured by ORIEL Corp. The light from the light source went through the monochromator and the wavelength of the incident light was adjusted to be 325nm by the monocharomator A. An optical filter was used in order to cut stray radiation from

the light source and scattered light from the samples. The PL from the sample was collected by a monochromator and the spectrum was recorded using a photomultiplier. The photon signals were converted into electrical signals by a picoammeter that is connected to a computer.
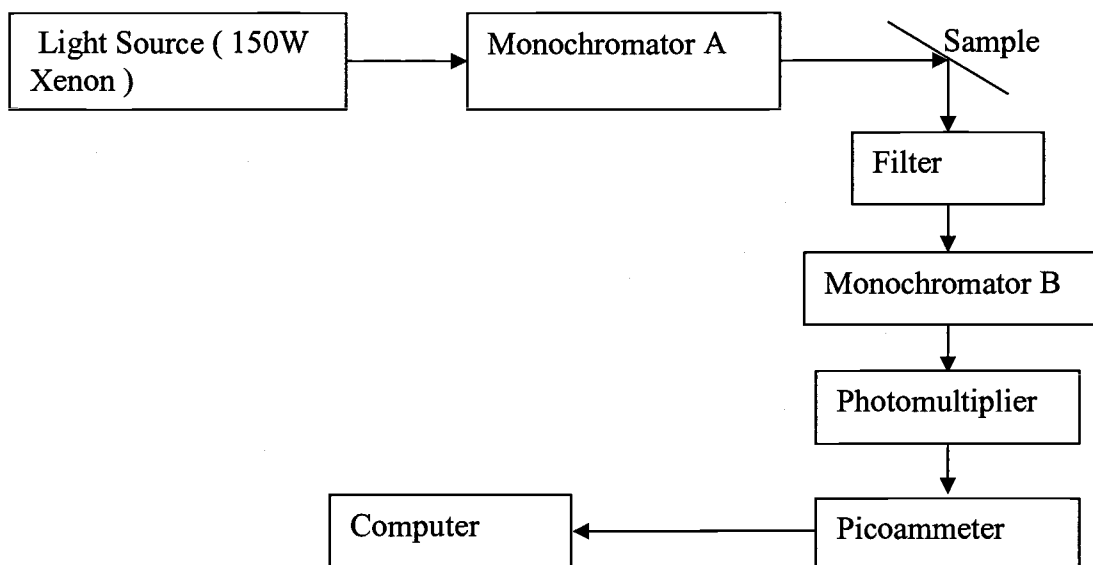
Fig.5 Schematic diagram of the apparatus for the measurement of photoluminescence

Chapter 4
Results and Discussion

This chapter will present the characterization results of diatom species, *Nitzschia frustulum,* including ICP, SEM-EDS, TEM-EDS, FT-IR, XRD and PL. The samples used for most characterizations include the original cell mass, and powder samples treated with H_2O_2, oxygen plasma, $800^{\circ}C$ thermal annealing, but some characterization only involved the samples treated with one or two of the methods mentioned above. The specific sample treatment methods will be emphasized for a particular characterization technique below.

The label of the sample name is explained here. All samples are labeled as "Ni22-5-1" or "Ni22-5a-1", where Ni represents the diatom species *"Nitzschia frustulum"*, 22 means the specific cultivation experiment number, 5 represnets the fifth sample of the 22nd experiment, (here it should be pointed out that the letter "a" means the sample was fed with germanium), and the last Arabia number 1 means the sample came from the first vial containing the sample taking out from the bioreactor.

4.1 ICP

The Table 1 gives the content of the major inorganic components in each sample. In order to measure the comparatively accurate content of every element, all samples are original green cell mass, without etching or annealing treatment. This avoided the possibility that some components could be diminished during etching or annealing treatment.

Table1 Metal content of diatom *Nitzschia frustulum* dry biomass

Sample	Metal (mg/g dry cell mass)		
	Ca	Si	Ge
Ni22-5-1	8.38±0.025	26.37±0.233	0
Ni22-7a-1 (1.92 hr)	8.61±0.015	27.39±0.401	5.00±0.405
Ni22-10a-1 (119.43 hr)	8.44±0.55	17.83±1.339	0.96±0.019

For ICP measurements, only three elements were tested, Ca, Ge and Si. Germanium is a small fraction of the total mass and the amount of Ge changes with time dramatically. Take sample Ni22 as an example, the content of Ge changes from 5.00 mg/g at 1.92 hour to 0.96 mg/g at 119.43 hour after addition of Ge. This implies that germanium was absorbed by diatom cells driving by the concentration difference initially and effluxed back to the bulk medium. Only a small fraction of germanium can be incorporated within the cells permanently.

The germanium absorption (or incorporation) patterns are different based on different cultivation process. By controlling the cultivation strategy, the germanium can be incorporated into the diatom cell permanently. This is illustrated in Clayton Jeffryes' MS thesis[5]. The ICP data for these samples listed in Table 1 is intended to show the rough contents of some major inorganic elements in diatom, but not to demonstrate the mechanism of germanium uptake which is detailed in Clayton Jeffryes' thesis.

4.2 SEM and TEM investigation

4.2.1 Frustule shape investigation

The cell mass of *N. frustulum*, was dried in air at room temperature, then treated with H_2O_2, oxygen plasma or thermal annealing. Finally, the carbonaceous materials were removed and a white powder was obtained from each treatment method. A SEM image of the cell mass without addition of germanium treated with H_2O_2 taken in Portland State University (PSU) is shown in Fig.6. The average pore size is about 200nm in diameter.
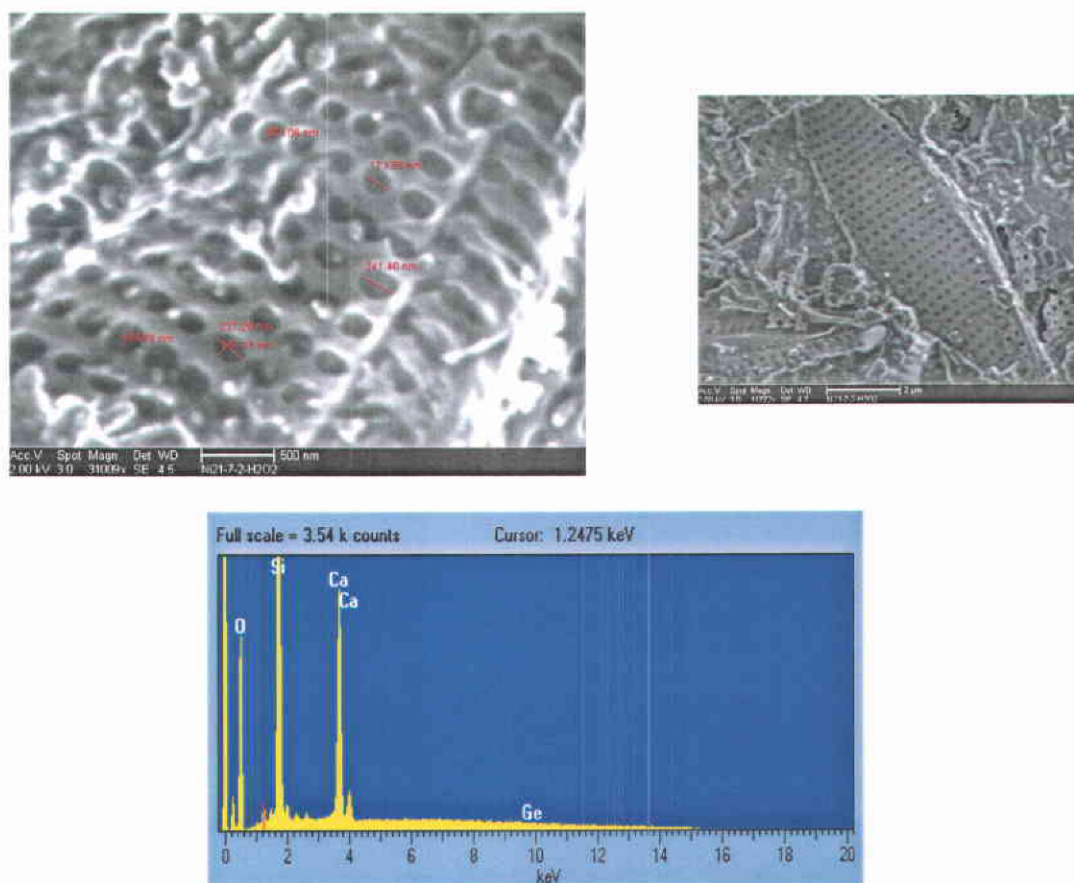

Fig.6 SEM-EDS of sample Ni21-7-2 treated with H_2O_2

The cell mass Ni22-10a-1 obtained 119hr after pulse addition of germanium to the Si-starved diatom cell suspension culture, treated with H_2O_2 was observed by SEM (PSU). The images are shown in Fig. 7.
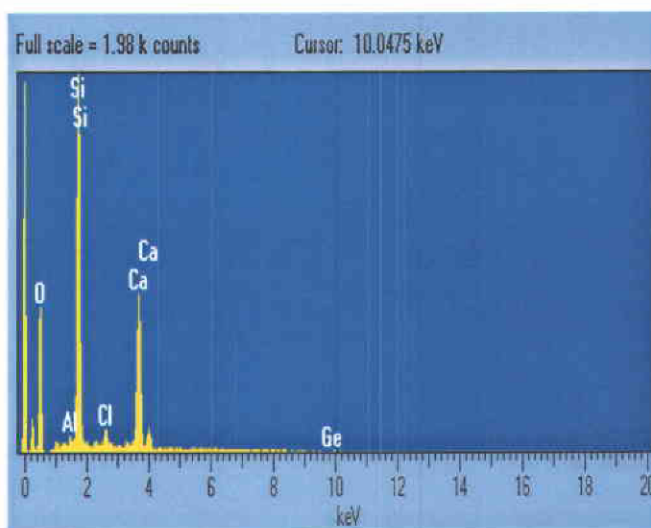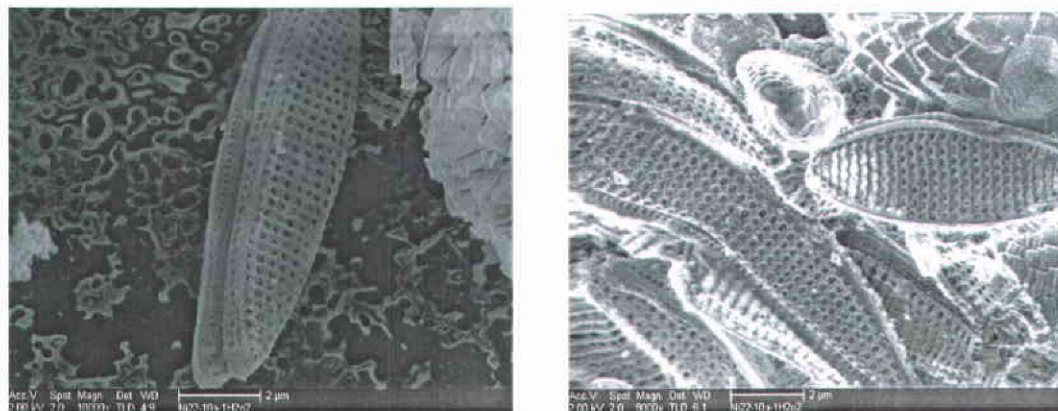

Fig.7 SEM-EDS of sample Ni22-10a-1 treated with H_2O_2

Both Fig.6 and Fig.7 show that diatom shell remained intact when the samples were treated with H_2O_2 no matter the sample was added with germanium or not. The

SEM images clearly show the surface structure featured with uniform distribution of pores and the pennate shape of the cell wall of diatoms, *Nitzschia frustulu*. The corresponding EDS spectra for the two samples show the similar results and no germanium signal was observed even for the sample with addition of germanium. This implies that the germanium was not dispersed on the surface of the cell wall.

Another SEM image of the cell mass (after annealing) taken in PSU is presented in Fig.8. Compared with Fig. 6 and Fig. 7, Fig. 8 shows the skeleton of diatom frustule, but the diatom shells did not remain their intact shape after thermal annealing. This reminds one that if it is very important to keep diatom shell intact, the samples should be treated with H_2O_2, but not with thermal annealing.
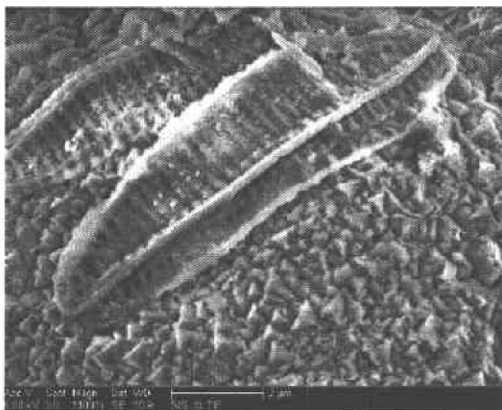

Fig.8 SEM image of annealed *N. frustulum* frustules

4.2.2 Composition analysis using TEM-EDS

In order to investigate the composition of the cell mass, TEM-EDS was used to analyze sample treated with H_2O_2 (sample Ni22-10a-1) and sample treated with

thermal annealing (sample Ni27-13a-3) at PSU. Fig. 9 shows the TEM image and EDS spectrum of sample Ni22-10a-1. Fig.10 shows the image of the annealed powder of sample Ni27-13a-3, and the EDS spectrum for which the X-ray collection was over the entire area of the material seen on the image. The atomic ratio of Si to Ge is around 5:1. It has to been noted that copper and carbon mainly come from the TEM grid. Unlike SEM-EDS analysis, from the TEM-EDS analysis of samples with addition of germanium no matter treated with H_2O_2 or treated with thermal annealing, both Fig. 9 and Fig.10 show the signals of germanium. This implies that germanium can be incorporated inside of diatom cells.
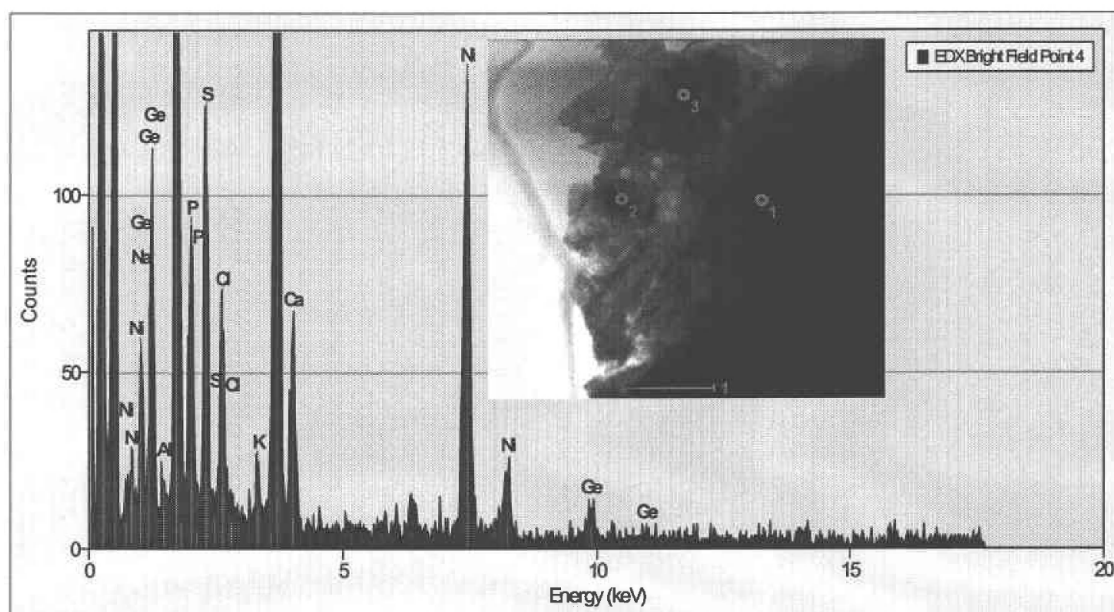

Fig.9 TEM-EDS analysis of sample Ni 22-10a-1 (H_2O_2 treated)
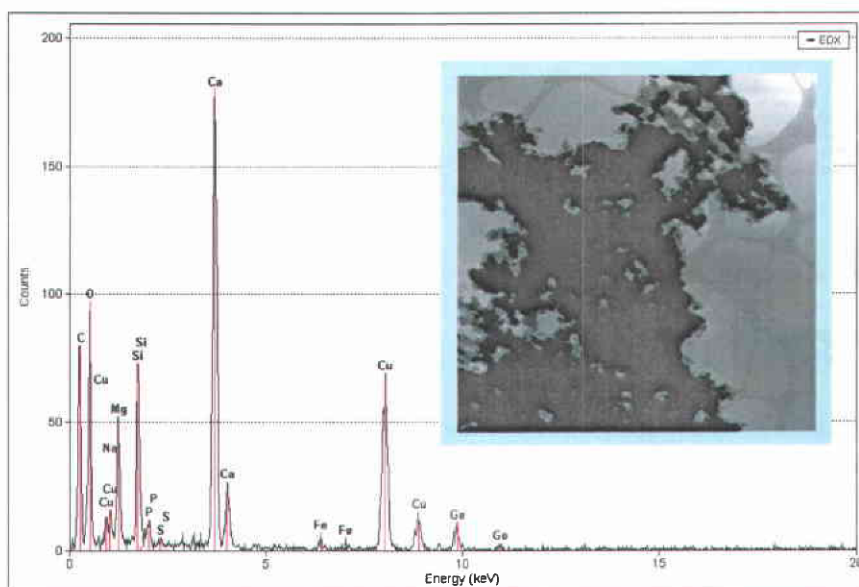
Fig.10 TEM-EDS analysis of sample Ni 27-13a-3 (annealing)

A TEM-EDS line scan through a representative nanocluster revealed nanostructured phases of Si and Ge (Fig.11). The material with the darker contrast tended to be richer in Ge, and the distribution of Ge is uniform along the scanning line. The quantitative elemental analysis of the nanocluster showed that 95 to 98% of the elemental constituents of the white powder were Si, Ge, Ca, Mg, and O. The atomic composition of oxygen was sufficient to ensure that all metals were in an oxide form.
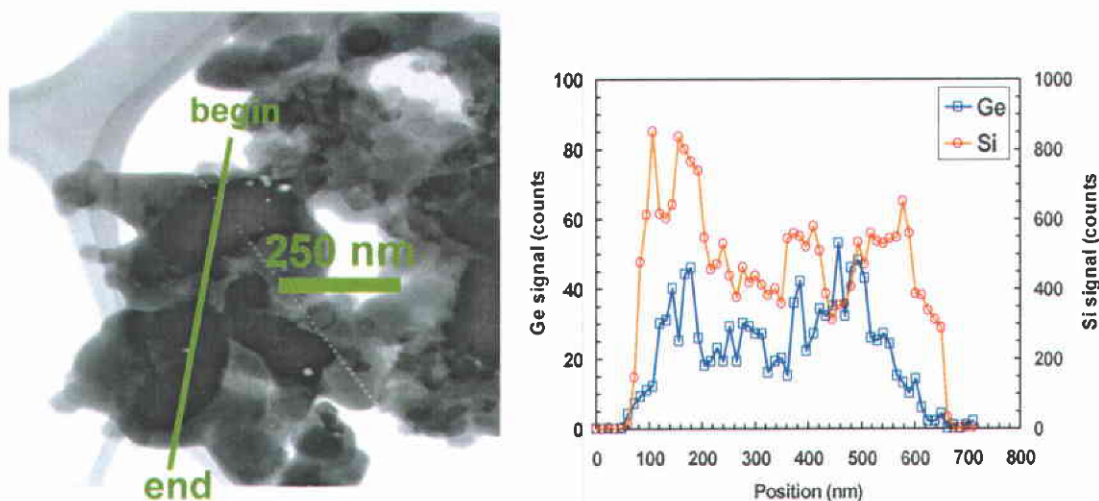
Sample preparation:
- **Thermal annealing of diatom cells (800 °C, 7 hr)**
- **Grind to powder**

Fig.11 Silicon and germanium distribution via TEM / EDS line scanning

4.2.3 Investigation of nanoparticles

The nanoparticles of SiO_2 were discovered by TEM-EDS analysis for almost every sample. Fig.12 shows a typical TEM image of SiO_2 nanoparticles and the corresponding EDS data for oxygen plasma treated sample Ni62-17a. Fig.13 is the high resolution TEM image of a typical nano-SiO_2 particle. Its size is around 30nm.
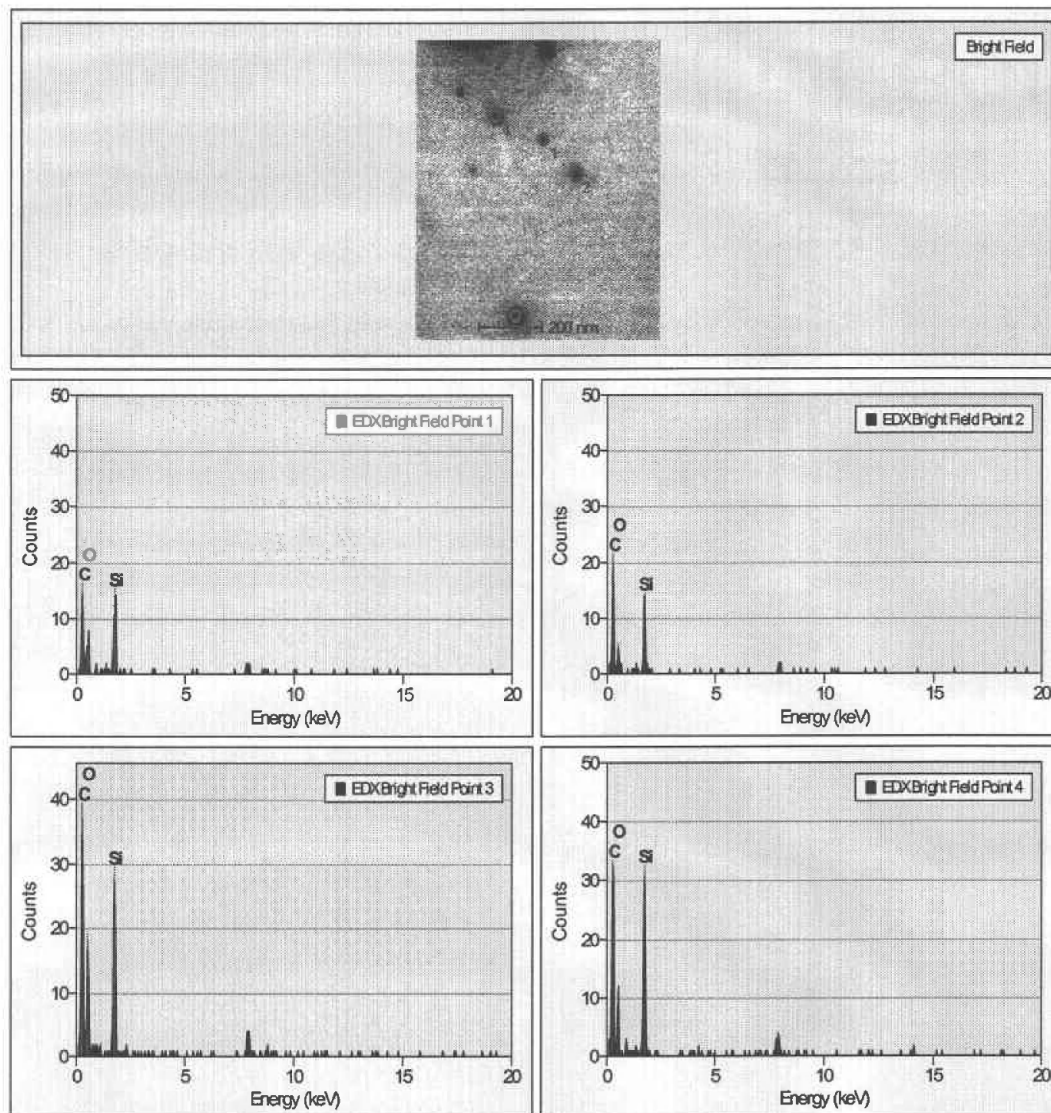
Fig.12 Nanoparticles of SiO$_2$ from etched sample Ni62-17a
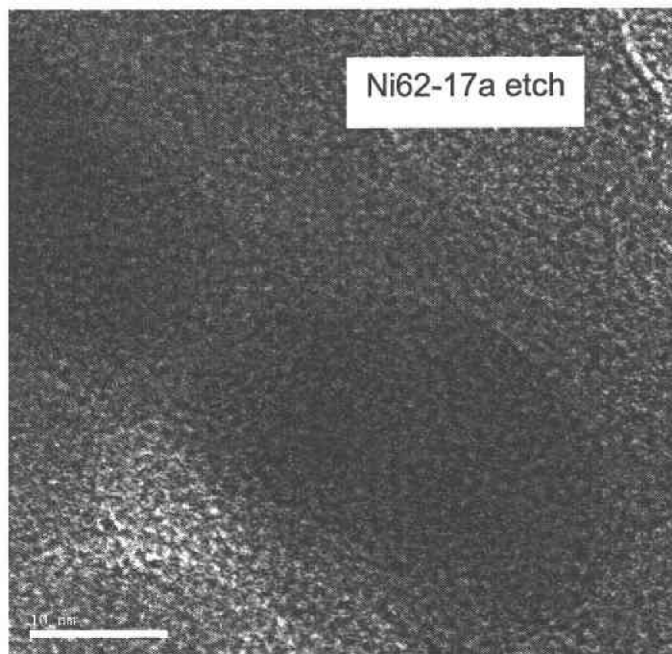
Fig.13 A typical nanoparticle of SiO_2 from etched sample Ni62-17a.

4.2.4 Determination of Ge location within diatom cell

From the study above, it is clear that germanium was incorporated into the cells. In order to determine where germanium is located, sliced samples prepared using microtome were observed under TEM. Fig.14 is the image of the cross section of a typical cell. EDS analysis shows that germanium signal can be seen only on the periphery indicated by arrow (include the whole inside periphery). When the probe was put on center and outside of the circle-like periphery, no germanium signal was observed. This is consistent with the SEM-EDS analysis shown previously that germanium signal was not observed on the surface of diatom shells.
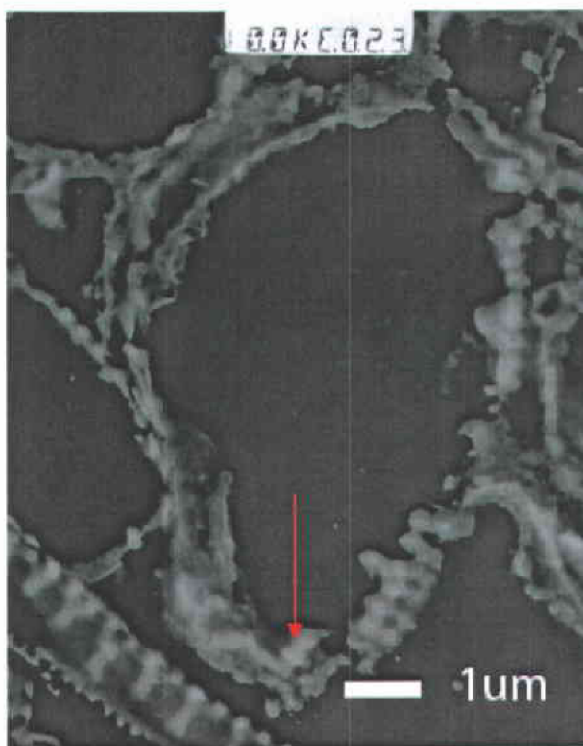
Fig.14 TEM image of cross section of a typical diatom cell

4.2.5 Other observations from TEM-EDS analysis

Interestingly, crystal form of titanium oxide was found in several samples, and one of the samples is Ni22-16a-7. The images are shown in Fig.15(a) and (b) and the corresponding EDS data is shown in Fig.15(c). It is speculated that the titanium came from the sea water, but apparently the titanium content in see water is very small (0.65 μg/litre)[25]. To explore where the titanium came from will be the topic worth doing more works in the future.
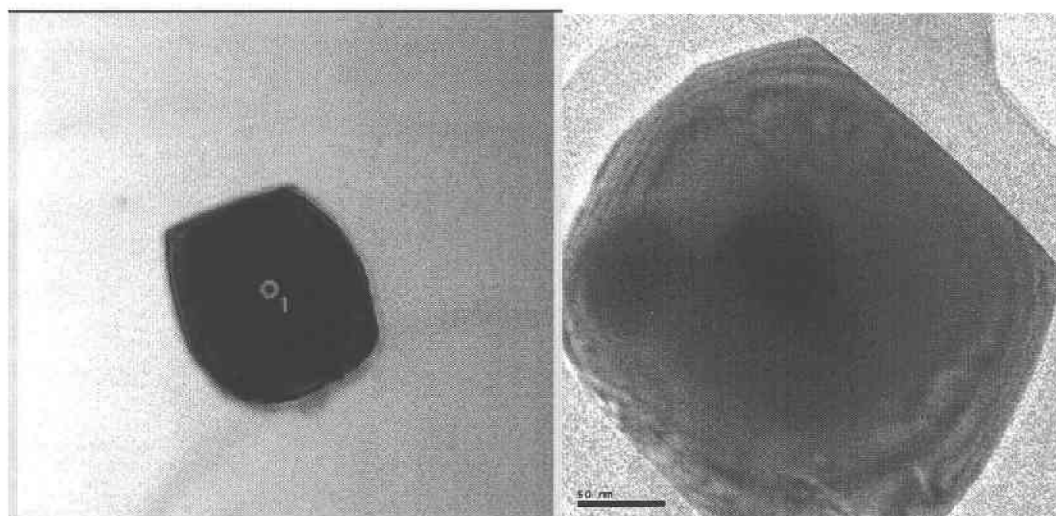
(a) (b)
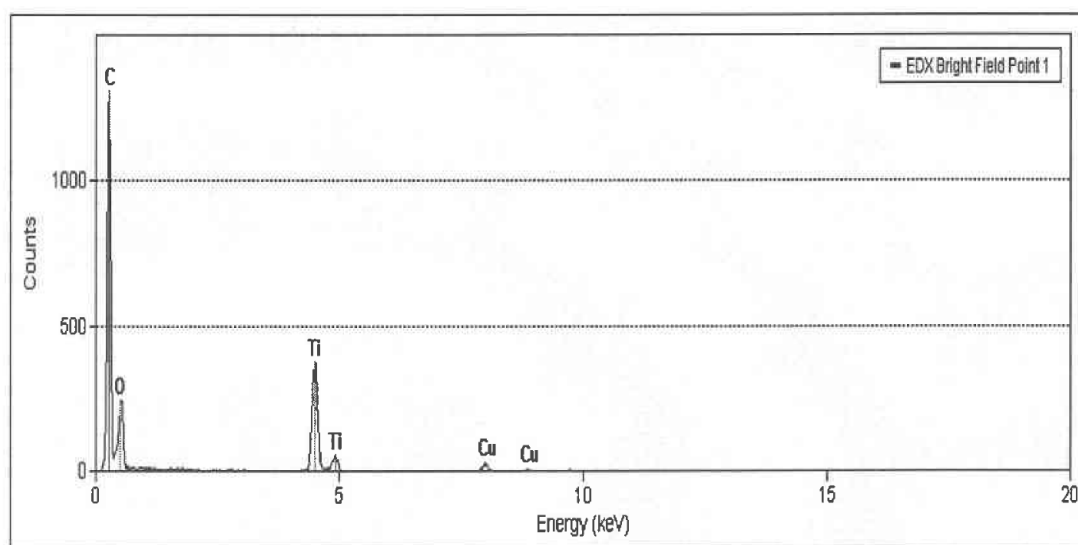
(c)

Fig.15 Observation of titanium oxide from sample Ni22-16a-7

4.2.6 Summary of SEM and TEM work

SEM analysis provided clear surface structure of the diatom shell; the typical pore size is about 200nm in diameter. If remaining the intact shell is required, the etching and thermally annealing methods seem not reliable methods to treat the diatom cell. However, the diatom shell could remain its intact shape, as long as the sample preparation procedure using H_2O_2 is carefully followed. TEM-EDS results show that germanium was incorporated into the cell and it is located on the inside perimeter edge of the shell. The typical amorphous nanoparticle of SiO_2 with 30nm diameter was observed. Crystal TiO_2 was observed for several samples and the origination of TiO_2 will be an interest topic for future work.

4.3 FT-IR

From the literature reports about infrared spectra of diatoms, we can conclude that the characteristic absorbance peaks of amorphous calcium carbonate (ACC), calcite (crystalline $CaCO_3$), and tetrahedron $[SiO_4]^{4-}$ are as follows:

ACC: $866cm^{-1}$(broad), $1086cm^{-1}$(broad), and $1420cm^{-1}$.[26]

ACC: $866cm^{-1}$(broad peak of carbonate bending), split at 1420 and $1474cm^{-1}$ (asymmetric stretch of carbonate ion)[27].

ACC: $1029cm^{-1}$ and $1082cm^{-1}$.[28]

Calcite: $713cm^{-1}$, and $875cm^{-1}$.[27]

The spectrum of tetrahedron $[SiO_4]^{4-}$ under CaO effect is complicated. In the CaO-SiO_2 silicate system, the spectrum is interpreted as the tetrahedron $[SiO_4]^{4-}$ vibration according to the ratio of NBO/Si (non-bridging oxygen per silicon) and the peaks at 1090, 990, 920and $870cm^{-1}$ are assigned to NBO/Si=1,2,3,4 respectively. The wavenumber of $1200cm^{-1}$ is assigned for $[SiO_4]^{4-}$ when NBO/Si=0, namely the fully polymerized units. The $480cm^{-1}$ stems from rocking of bridging oxygen in a fully polymerized three- dimensional network and it disappears when the composition of CaO is greater than 44.1% CaO^{29}. The schematic illustration for tetrahedron $[SiO_4]^{4-}$ structural units with NBO/Si=1,2,3,4 is shown in Fig.16.

```
              |                              |
              Si                             Si
              O                              O
              |                              |
  — SiO — Si — O⁻              — SiO — Si — O⁻
              |                              |
              O                              O⁻
              Si
              |

        NBO/Si=1                      NBO/Si=2


              O⁻                             O⁻
              |                              |
  — SiO — Si — O⁻         O⁻ — Si — O⁻
              |                              |
              O⁻                             O⁻

        NBO/Si=3                      NBO/Si=4
```
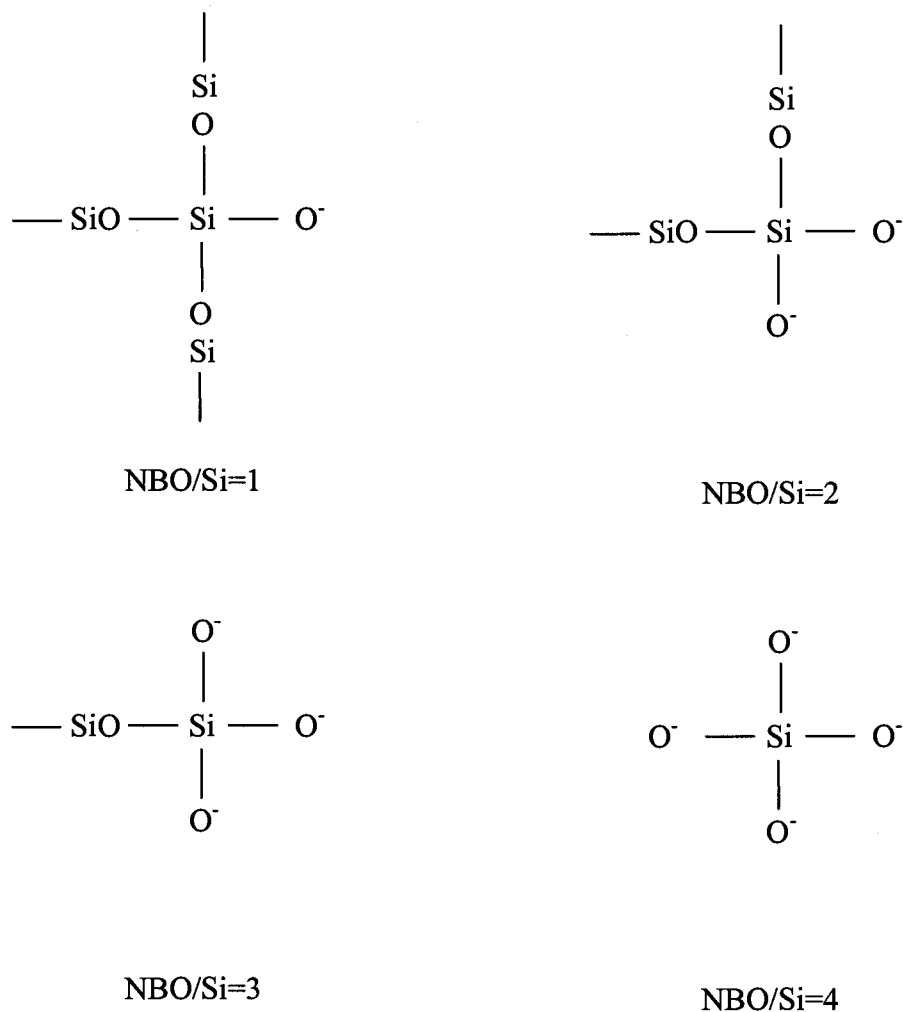
Fig.16 schematic illustration of tetrahedron $[SiO_4]^{4-}$ structural units

Compared the FT-IR data in literature reports with the FT-IR results of diatom species, *Nitzschia frustulum*, here we figured out its compositions.

4.3.1 FT-IR results of the diatom samples without the addition of germanium

Fig.17 shows typical FT-IR spectra of diatom sample without the addition of germanium. The two spectra represent sample Ni22-5-1. One of them is the original dried cell mass without any further treatment, original Ni22-5-1. The other one is the sample treated with oxygen plasma, etched Ni22-5-1. Compared the two spectra, we

can see the number of the absorption peaks of the etched sample is less than that of the original sample. In addition, some peak shifting was observed after oxygen plasma treatment. This is caused by removing the organic materials. Based on the reported FT-IR data, the sample, Ni22-5-1, mainly consists of amorphous calcium carbonate (1420 and 1084cm^{-1}), calcite (874 and 714cm^{-1}) and $[SiO_4]^{4-}$ (Si-O rocking band at 465cm^{-1}, which is a little bit different than 480cm^{-1} reported in literature but consistent with the experimental data conducted in this thesis. (The spectrum of amorphous SiO_2 is shown in Fig.19.)

In order to obtain an accurate FT-IR analysis, a number of samples without the addition of germanium were treated. All samples show very similar spectra. Here we present spectra from two samples to show the reproducibility. Fig.18 shows the FT-IR spectra from another sample, Ni26-4-3.
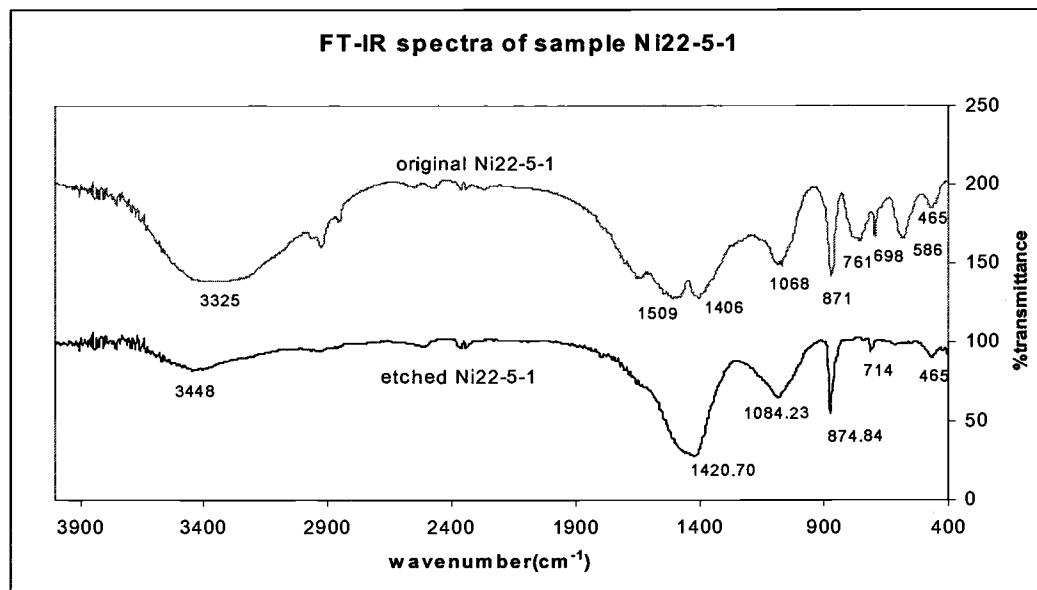

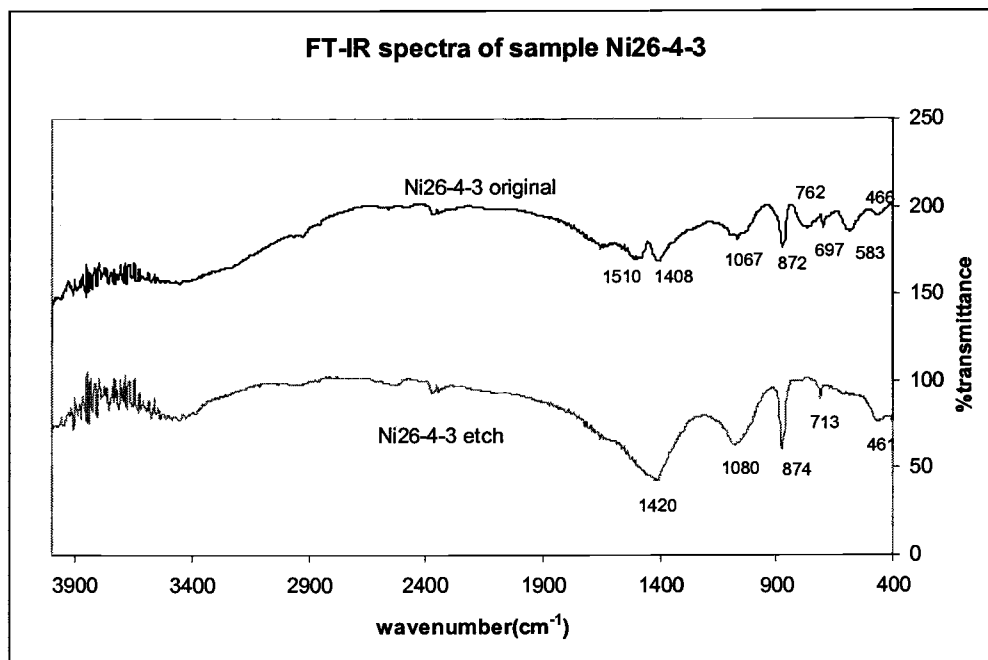
Fig.17 FT-IR spectra of sample Ni22-5-1

Fig.18 FT-IR spectra of sample Ni26-4-3
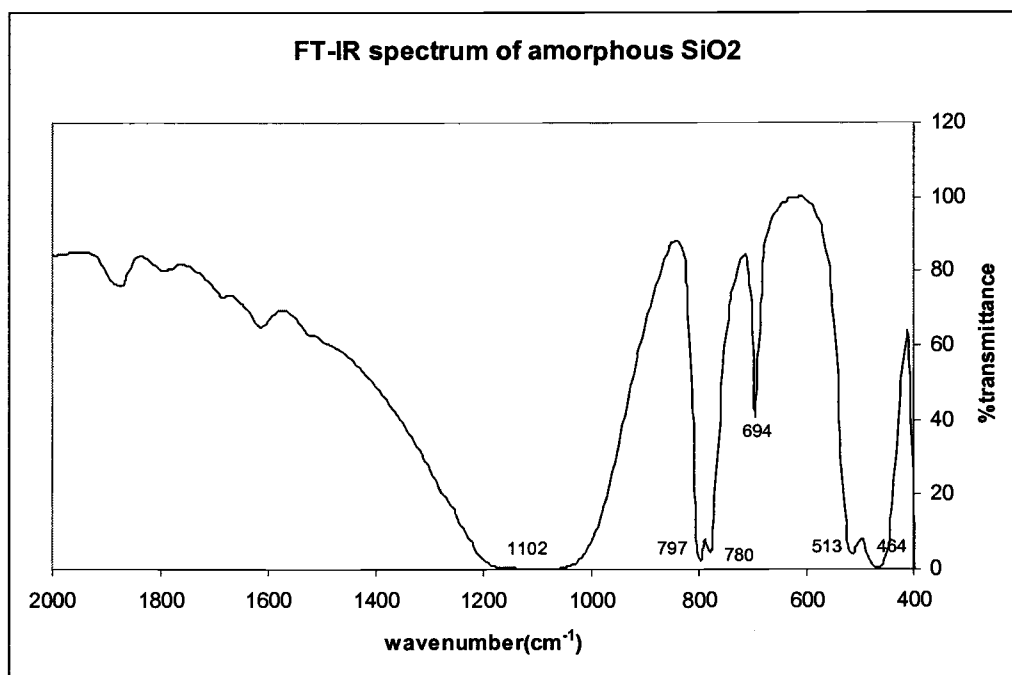
Fig.19 FT-IR spectrum of amorphous SiO_2

4.3.2 FT-IR analysis before and after adding germanium

Fig.20 and Fig.21 show the FT-IR spectra of etched samples Ni22 and Ni23, respectively. Both spectra show a partial region of FT-IR spectrum results of the sample before and after adding germanium. The most obvious difference between the samples before and after adding germanium is shown around wavenumber of 870cm^{-1}. After adding Ge for a comparatively long time, for sample Ni22-10a-1, the 870cm^{-1} peak disappeared and the 853cm^{-1} peak became very strong. We believe this change is related to germanium. It was reported that germanium dioxide has an absorption peak at 850cm^{-1}.[30] In order to confirm this peak, several repetitions of FT-IR scan of sample Ni22-10a-1 were done with good reproducibility.
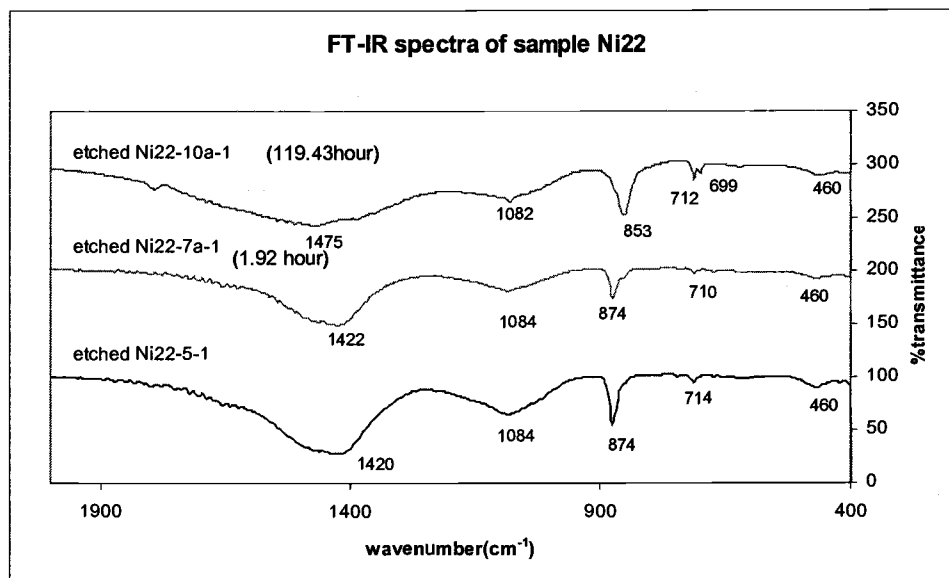
Fig.20 FT-IR spectra of sample Ni22 before and after adding Ge

FT-IR of Ni23-5-1etch

FT-IR of 23-7a-1etch (17.02hr)

FT-IR of Ni23-9a etch (109.77hr)
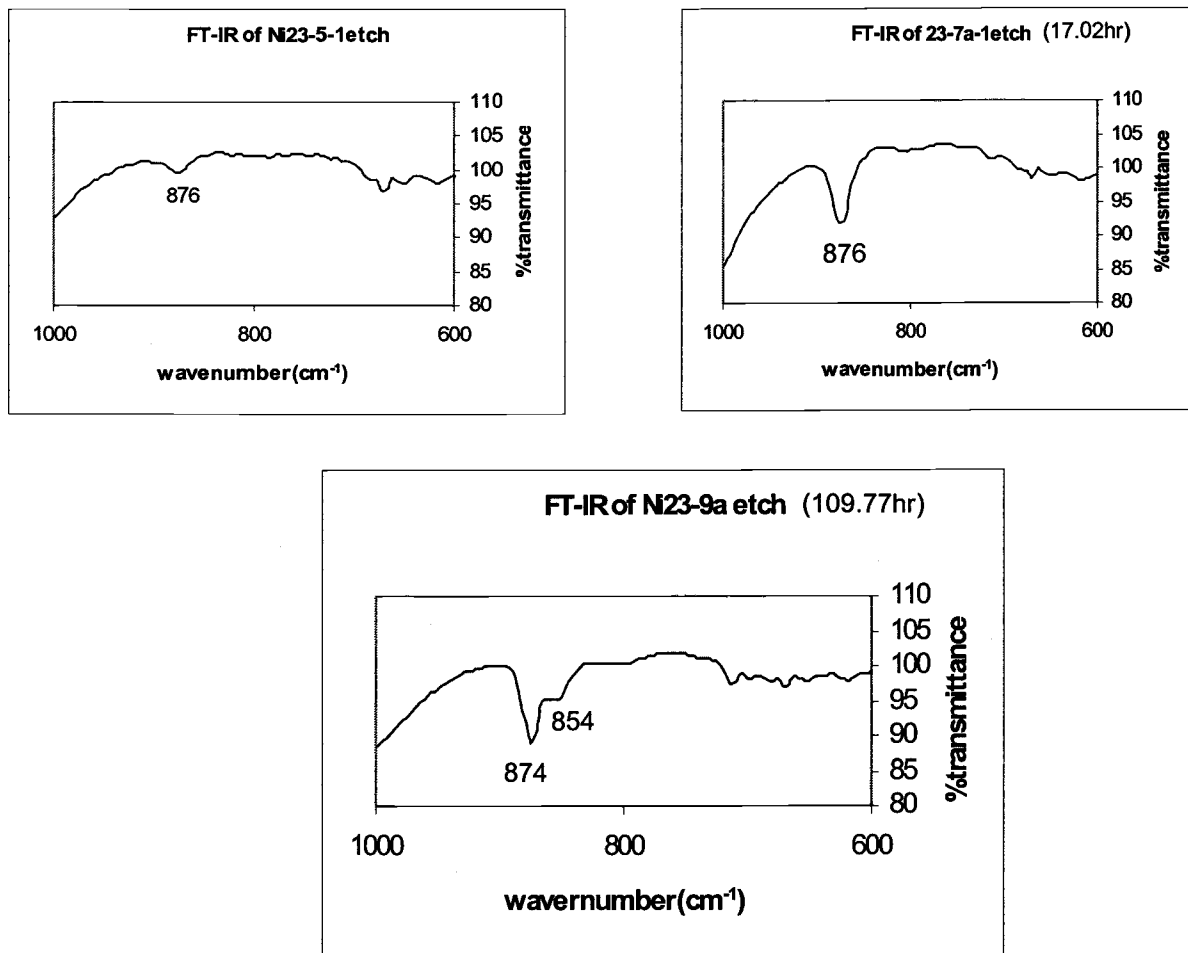
Fig.21 FT-IR spectra of sample Ni23 before and after adding Ge

4.3.3 FT-IR analysis of samples after 800°C annealing

Fig.22 shows the FT-IR spectra of diatoms after 800°C annealing. Compared this result with that reported data, we can see that during annealing, $CaCO_3$ is converted to CaO and interacted with SiO_2, furthermore non-bridging oxygen (to silicon) is increased. This is reflected from the peaks at 990 and $920cm^{-1}$, which were assigned to NBO/Si=2,3 respectively. We propose that the peak around 1120 cm^{-1} is related to

NBO/Si=1, however it is different from1090 cm^{-1} that was reported in literature. The possible reason for this is the effect coming from some other materials in diatom (such as Mg, Fe). At 4 hrs after Ge addition (Ni27-7a-3 annealed 7hr), the uptake of soluble Ge by the diatom cell suspension culture was near its maximum[31], however the FT-IR spectrum of the thermally annealed biomass was similar to the thermally annealed cell mass before Ge addition, indicating that Ge was not yet incorporated into the diatom cell and washed away during sample praperation. However, at 123 hours after Ge addition (Ni27-12a-3 annealed 7hr), the FT-IR spectrum of the thermally annealed cell mass was quite different, as evidenced by the decrease of the peak intensity and the peak shifting around 920 cm^{-1}. These changes are speculated to be related to the addition of Ge, because the addition of Ge will distort the electronic environment of the original $[SiO_4]^{4-}$ network.
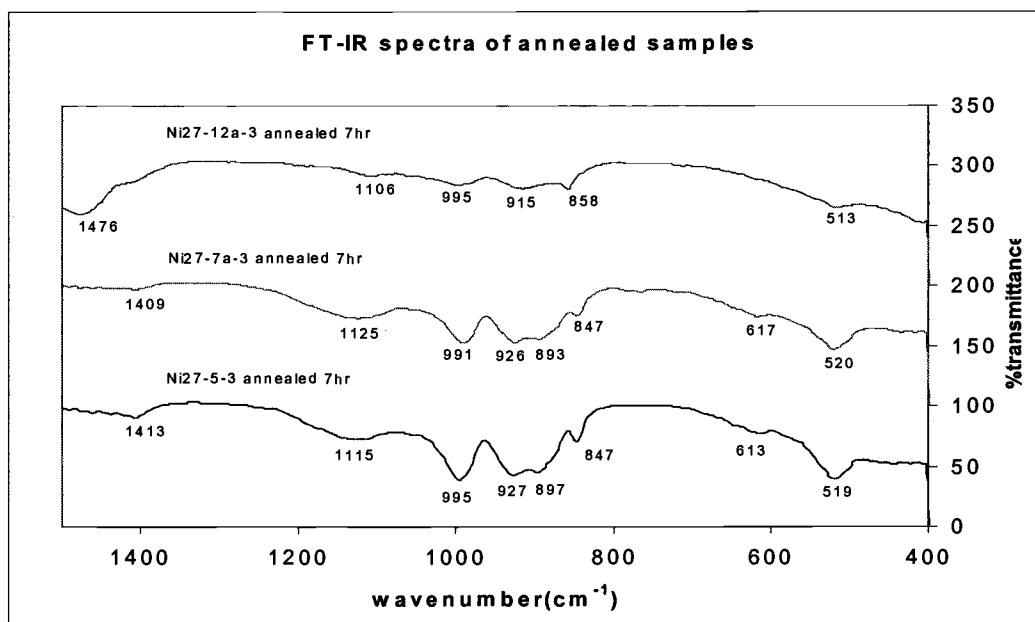

Fig.22 FT-IR spectra of annealed samples

By comparing Fig. 20 (for etched samples) and Fig. 22 (for annealed samples), we can obtain important information. In Fig. 20, the peak at 460cm^{-1} stems from rocking mode of Si-O in a fully polymerized (NBO/Si=0), three-dimensional network of [SiO$_4$]$^{4-}$. [29] However, in Fig. 22, the peak at 460cm^{-1} is disappeared and replaced by peak 520cm^{-1} which is assigned to the bending mode of Si-O bonds[29]. The bending mode of Si-O bonds usually accompanies with the appearance of nonbridging oxygen. This result reflects that no solid reactions happened during oxygen plasma treatment process, but some solid reactions occurred when samples were treated with 800°C thermal annealing. Those solid reactions caused the appearance of non- bridging oxygen (to silicon).

4.3.4 Summary of FT-IR results:

FT-IR is a useful tool to characterize the chemical bonding of the materials. Peak changes after the addition of germanium could be observed for both treatment of oxygen plasma and 800°C thermal annealing. However, the differences in certain wavenumber regions are not clearly distinguishable because of low germanium content.

The oxygen plasma treatment is an efficient method to study the original bonding information of diatoms. The FT-IR spectra of etched samples showed the existence of GeO$_2$, amorphous calcium carbonate, calcite and fully polymerized (NBO/Si=0), three dimensional [SiO$_4$]$^{4-}$ network in diatom samples with the addition of germanium.

FT-IR spectra of samples treated with $800^\circ C$ thermal annealing can show some differences after addition of germanium, but this treatment can cause some solid reactions and the original chemical bonding can be destroyed.
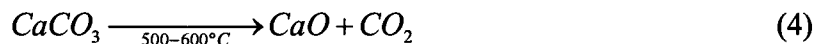
4.4 XRD

XRD was used to characterize samples with and without the addition of germanium. Most samples were subjected to thermal annealing to convert amorphous materials to crystalline phases therefore can be distinguished by XRD.

4.4.1 XRD analysis for samples without germanium

The XRD data for different samples are shown in Fig.23 to Fig.26. The XRD spectra indicated that the annealed diatom samples without the addition of germanium consist of $Ca(OH)_2$, $CaCO_3$, CaO, and Ca_2SiO_4, at different amount. For example, sample Ni29-6 and Ni30-6 contain mostly CaO, and Ni24-6 has more $CaCO_3$ and $Ca(OH)_2$. Calcium exists in these different forms, because $CaCO_3$, CaO and $Ca(OH)_2$ can be converted to each other under proper conditions.

$$CaCO_3 \xrightarrow[500-600°C]{} CaO + CO_2 \tag{4}$$

$$CaO + CO_2 \rightarrow CaCO_3 \tag{5}$$

$$CaO + H_2O \rightarrow Ca(OH)_2 \tag{6}$$

Under standard condition (temperature T=25°C, pressure P=1atm), for reaction (4):

$$\Delta S_1° = [(1 \text{ mol})(39.7 \text{ J/(K· mol)}) + (1 \text{ mol})(213.6 \text{ J/(K · mol)})]$$
$$- (1 \text{ mol})(92.9 \text{ J/(K · mol)}) = +160.4 \text{ J/K}$$

$$\Delta H_1° = [\Delta H°_f(CaO) + \Delta H°_f(CO_2)] - \Delta H°_f(CaCO_3)$$
$$= [(1 \text{ mol})(-635.1 \text{ kJ/mol}) + (1 \text{ mol})(-393.5 \text{ kJ/mol})]$$
$$- (1 \text{ mol})(-1206.9 \text{ kJ/mol}) = +178.3 \text{ kJ}$$

$$\Delta G_1° = \Delta H_1° - T\Delta S_1° = 178.3 \text{ kJ} - (298 \text{ K})(0.1604 \text{ kJ/K}) = +130.5 \text{ kJ} > 0,$$

so reaction (4) is nonspontaneous at standard conditions. This implies that the reverse

reaction (5) is spontaneous at standard condition. When the furnace temperature

reaches 800°C, reaction (4) happens.

For the reaction (6),

$$\Delta G_2^o = \Delta G^o_{f,Ca(OH)2\ (s)} - (\Delta G^o_{f,CaO\ (s)} + \Delta G^o_{f,H_2O\ (l)})$$
$$= -896.76 kJ/mol - (-604.2 kJ/mol\ -237.18 kJ/mol)$$
$$= -55.38 kJ/mol < 0$$

so the reaction (6) is a spontaneous reaction at standard condition.

If XRD tests were run for samples immediately taken off from the furnace, such as

Ni29-6 and Ni30-6, most calcium should be in the form of CaO. Fig.24 and Fig.25

illustrated this. The XRD spectra would show more $Ca(OH)_2$ and $CaCO_3$ if the tests

were run after the samples were exposed to air for a while, such as sample Ni24-6.

This is because CaO is exposed water and CO_2 in air and converted to $Ca(OH)_2$ and

$CaCO_3$. Fig.26 confirmed this.

XRD for samples without Ge

Ni30-6

Ni29-6

Ni24-6

10 15 20 25 30 35 40 45 50 55 60

2 theta
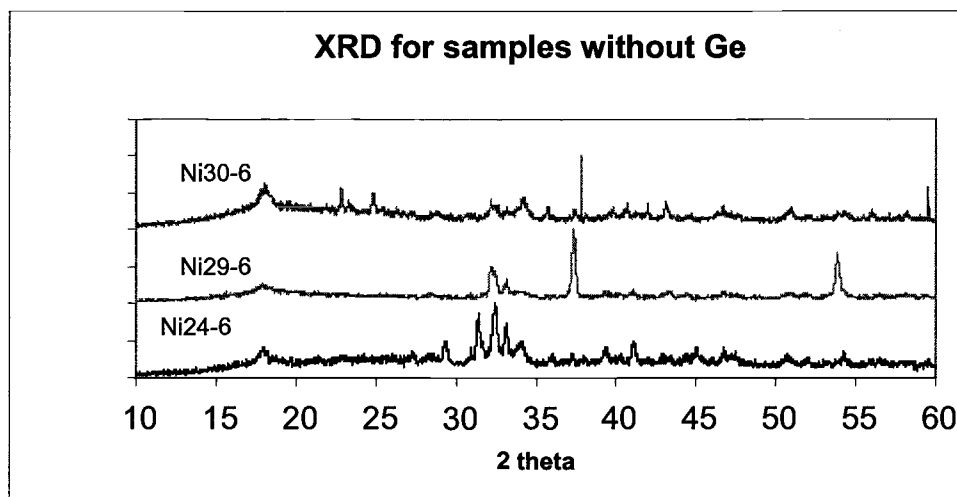
Fig.23 XRD for annealed samples without Ge
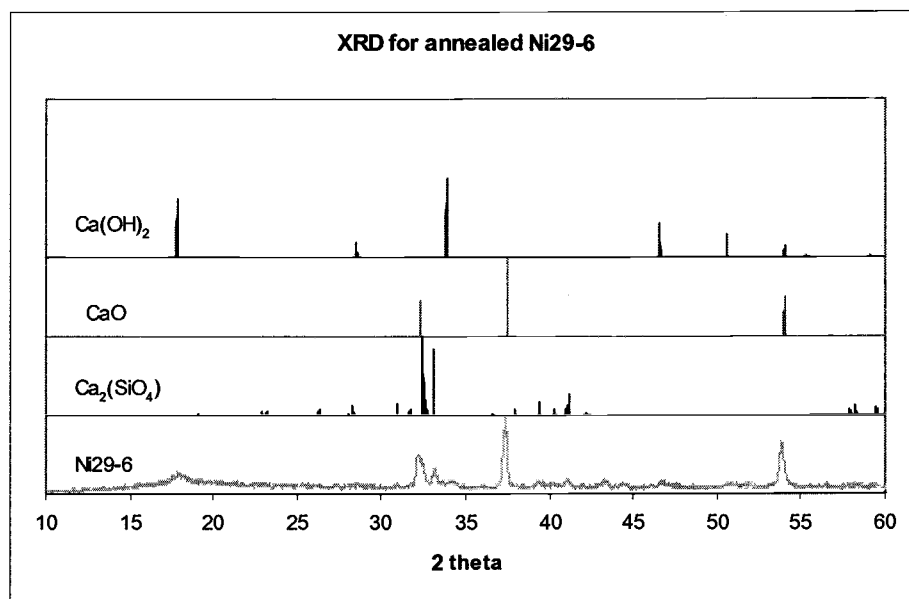
Fig.24 XRD for annealed sample Ni29-6
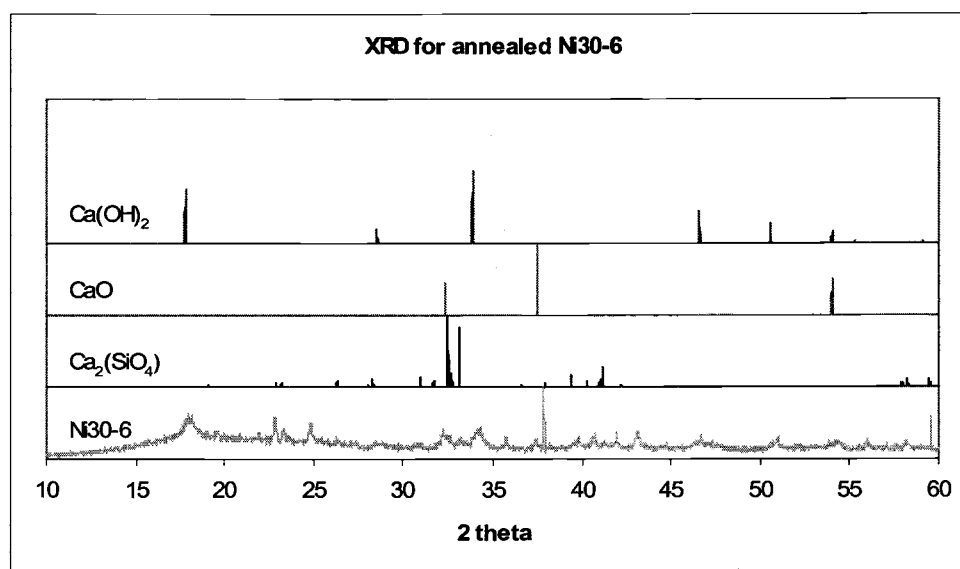
Fig.25 XRD for annealed sample Ni30-6
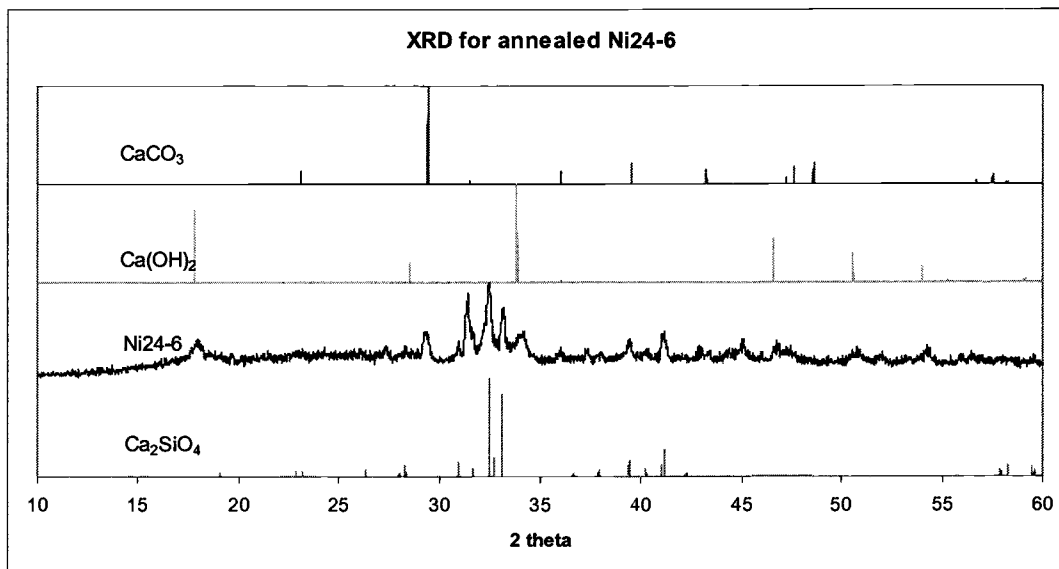
Fig.26 XRD for annealed sample Ni24-6

4.4.2 XRD analysis for samples with germanium

In comparison with the sample without germanium, the samples with germanium contain different phases. Calcium existed in a form of $CaSiO_3$ instead of Ca_2SiO_4 for all samples after adding germanium. Ca_3GeO_5 signals appeared in sample Ni36-16a-2 (Fig.27). The following mechanism could explain these differences. Under thermal annealing, CaO produced from $CaCO_3$. For samples without germanium, CaO would react with SiO_2 and form Ca_2SiO_4 according to:

$$2CaO + SiO_2 \rightarrow Ca_2SiO_4 \qquad (7)$$

When the sample contains germanium, part of the CaO reacted with SiO_2 and part of it reacted with GeO_2. The reactions are as follows.

$$CaO + SiO_2 \rightarrow CaSiO_3 \qquad (8)$$

$$3CaO + GeO_2 \rightarrow Ca_3GeO_5 \qquad (9)$$
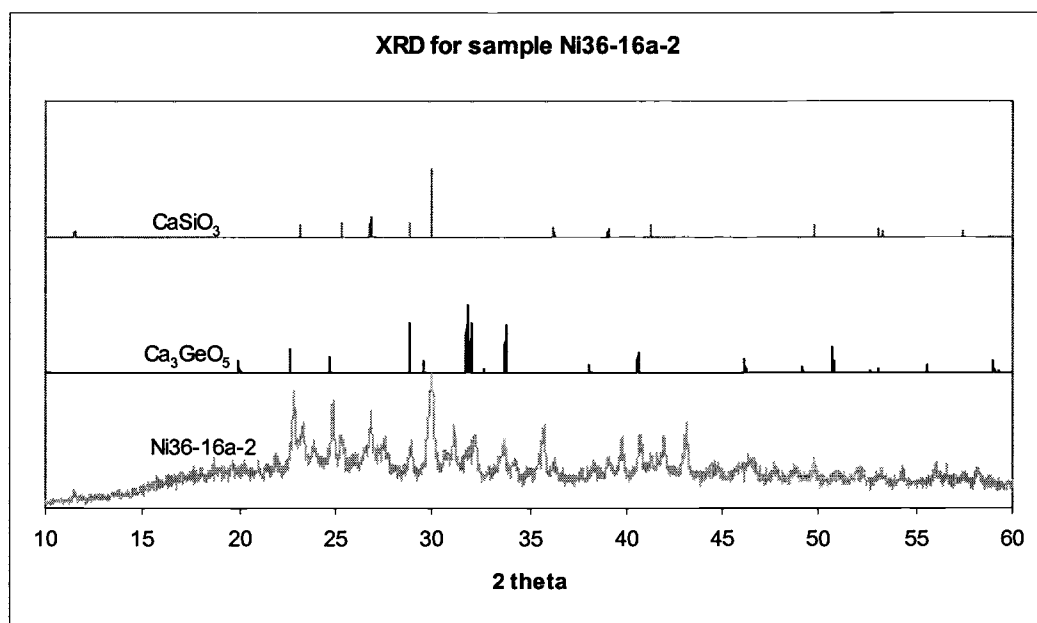
Fig.27 XRD for annealed sample Ni36-16a-2

The XRD spectra of samples with and without germanium are given in Fig.29. The three diffraction peaks at a 2θ value of 28.86, 31.8, and 33.76 match well with Ca_3GeO_5.
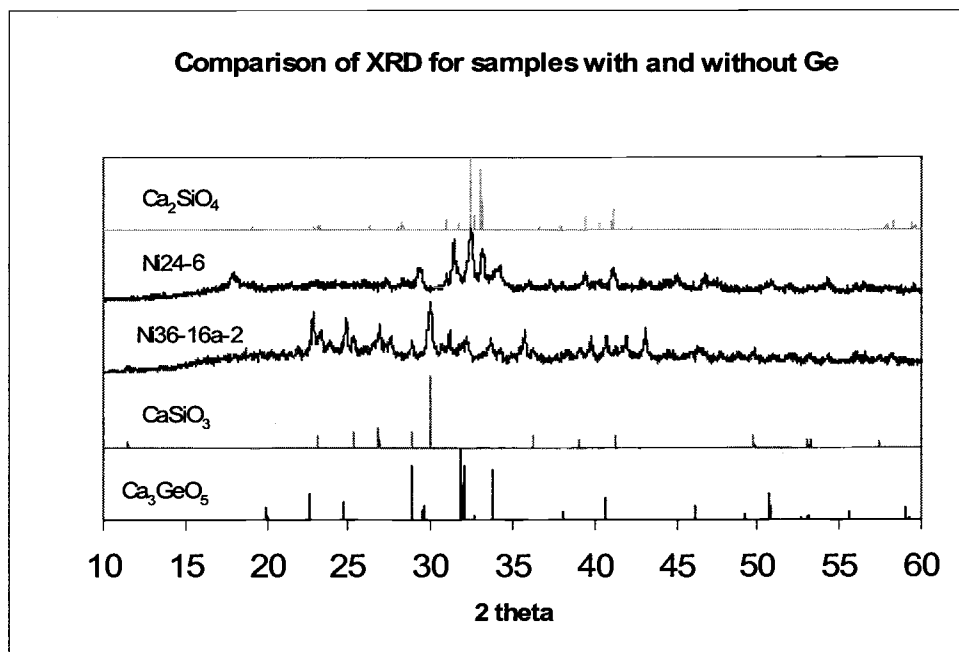
Fig.28 XRD for annealed samples with and without germanium

4.4.3 Summary of XRD results

XRD spectra of diatom samples with and without the addition of germanium that subjected to different treatments contain useful information. The annealing treatment induced the formation of crystalline phases. Some constitutes were converted to different materials after annealing. For example, $CaCO_3$ was converted to CaO or $Ca(OH)_2$; SiO_2 was converted to Ca_2SiO_4 in samples without the addition of germanium, to $CaSiO_3$ and Ca_3GeO_5 in samples with addition of germanium. The Ca_3GeO_5 signal indicated the existence of germanium. Although some conversions happened after thermal annealing, the treatment of thermal annealing is an effective way to help characterize the diatom material by XRD. The existence of GeO_2 in diatom cells could be verified from an indirect perspective.

4.5 Photoluminescence (PL)

Three kinds of powder samples treated with H_2O_2, oxygen plasma, and thermal annealing were used to study the photoluminescent property of diatom cells. The purpose of using different treatment methods is to know if the treatment method could affect the PL. Also the samples with and without adding germanium were tested to compare the difference of the PL. The PL emission spectra are shown as follows. All PL spectra were corrected for the system response. The image in Fig.29 shows the strong blue emission from sample Ni22-10a-1 treated with H_2O_2.

Fig.29 Blue emission from sample Ni22-10a-1 treated with H_2O_2

4.5.1 Emission spectra of samples treated with H_2O_2

Fig.30 shows the PL spectra of two samples without the addition of germanium treated with H_2O_2. They are very similar to each other. Each spectrum has a peak centered at 480nm, which is greenish blue color in the visible region.

Emission spectra of samples without addition of Ge
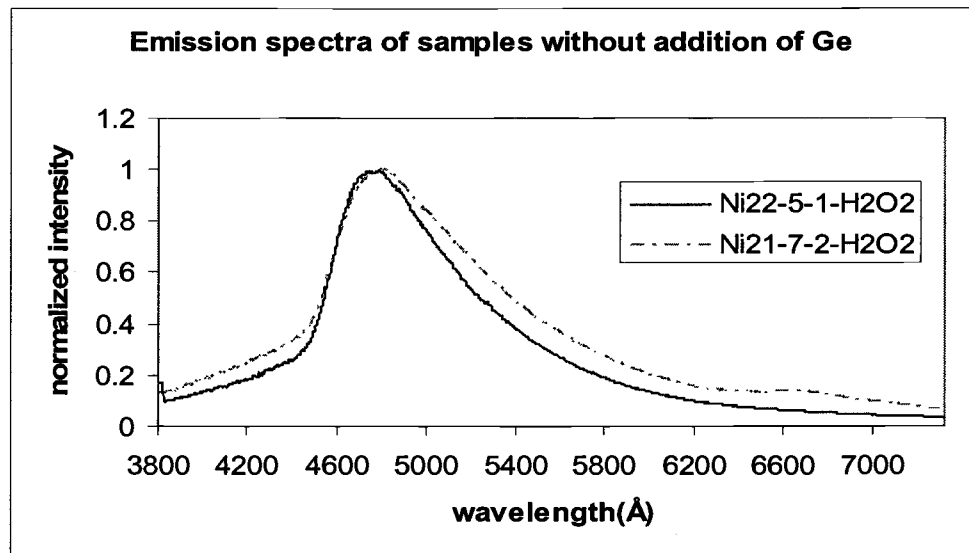
Fig.30 Emission spectra of samples without germanium

Fig.31 illustrates the emission spectra of two samples with addition of germanium. They are very similar, and the center peaks are located at 420nm and 430nm respectively. The color of the emission is blue. Fig.32 provides the comparison of the emission spectra of the sample Ni22 before and after adding germanium. Fig.32 clearly shows that the emission light of the sample with the addition of germanium is shifted to a higher energy (lower wavelength, called blueshift).
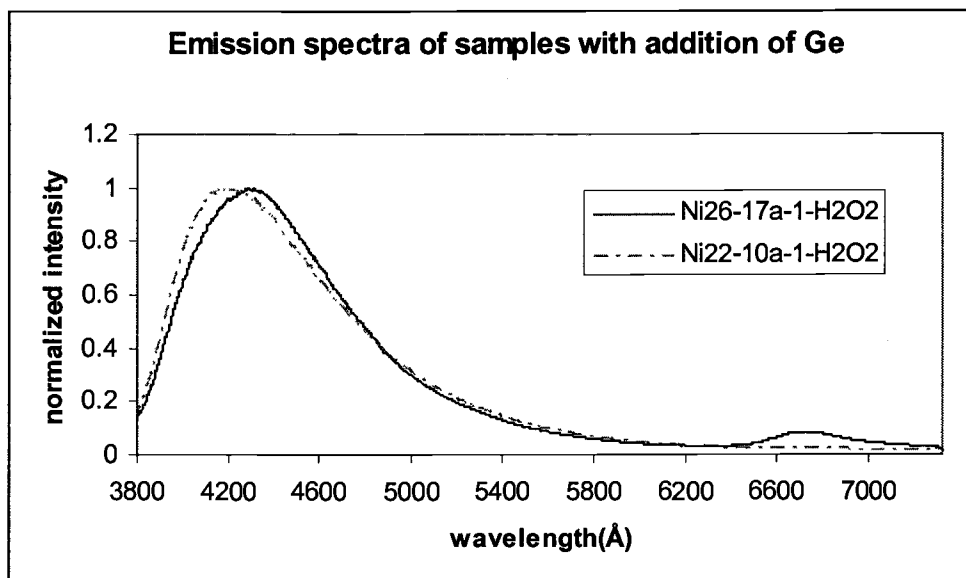
Fig.31 Emission spectra of samples with addition of germanium
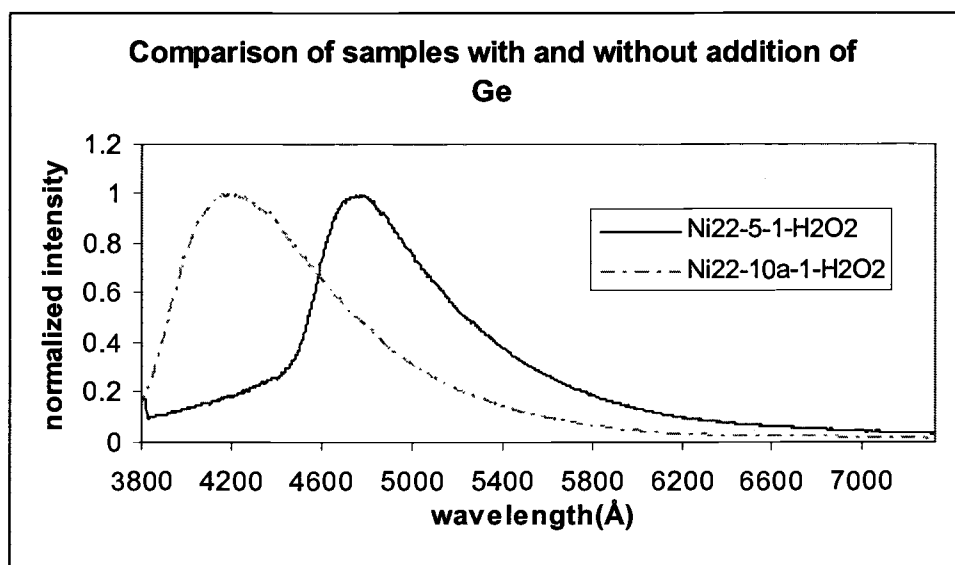
Fig.32 Comparison of emission spectra of samples before and after adding Ge

4.5.2 Emission spectra of samples treated with oxygen plasma

Fig.33 shows very similar emission spectra for three samples treated with oxygen plasma, no matter the sample has germanium or not. All of them have a broad peak located around 430nm, which gives blue visible light.

Emission spectra of etched samples
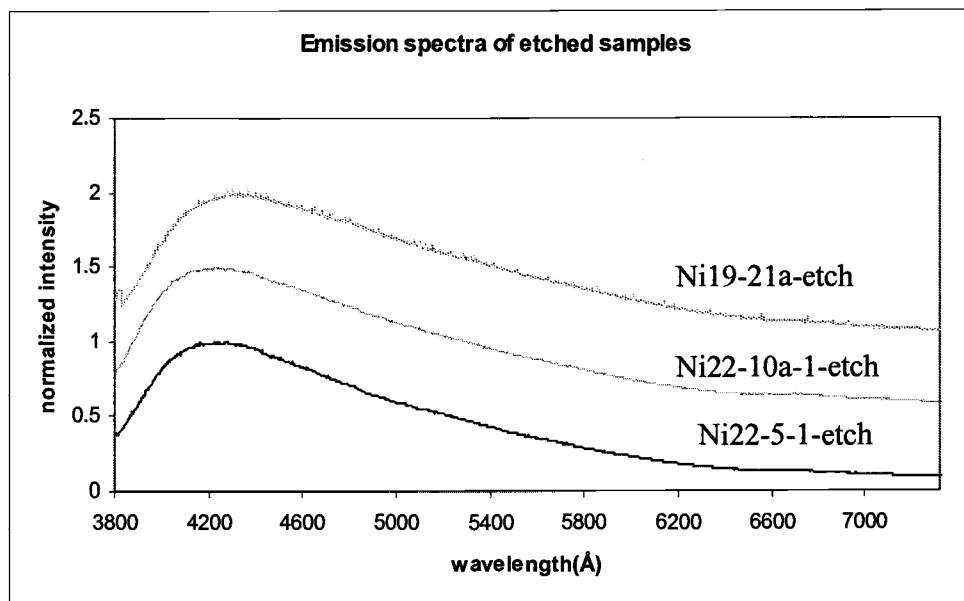
Fig.33 Emission spectra of etched samples

4.5.3 Emission spectra of diatom samples after 800°C annealing

Unlike the spectra of samples treated with H_2O_2 and oxygen plasma, all the samples after 800°C annealing (regardless of addition of germanium or not) showed no visible photoluminescence when they were excited by light with wavelength of 335nm. The spectrum of sample Ni22-5-1 annealed at 800°C is shown in Fig.36.

4.5.4 Influence of HF treatment on the emission spectra

In order to better understand the mechanism of photoluminescence originated from diatom samples, to know whether the size of the pores on the surface of the cell wall

contributes for the photoluminescence or not, the etched sample Ni22-5-1-etch was treated with HF. The treatment process is as follows: the etched Ni22-5-1 powder was dispersed into 48% HF for 20 minutes, the suspension was centrifuged for 10 minutes, pour the supernatant out, use deionized water to wash the left powder for 3 times, and finally dry the washed powder.

Fig.34 shows no distinguishable difference for sample Ni22-5-1-etch after HF treatment. This implies two possibilities: one is the HF treatment did not change the size of the pores on the surface of the cell wall of the etched sample within the short 30minutes, so there is no change on the photoluminescence; the another one is that the size of the pores has been changed, however, the size of the pores does not affect the photoluminescence.
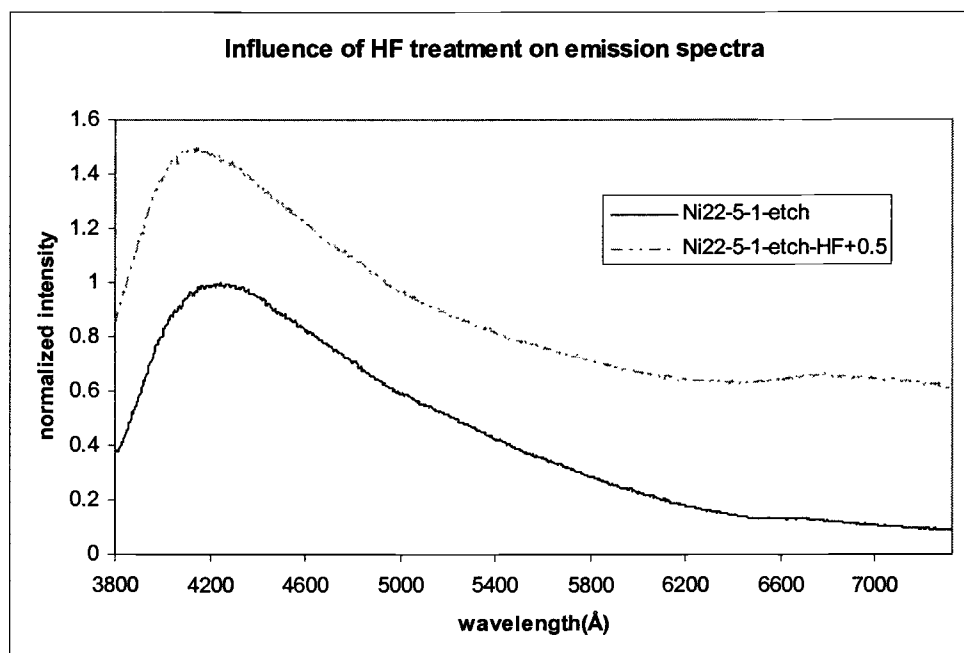
Fig.34 Influence of HF treatment on photoluminescence

4.5.5 Comparison of emission spectra of diatom samples and bulk amorphous SiO_2

It should be meaningful to compare the photoluminescent property of diatom samples with that of bulk amorphous silica (SiO_2), because the major component of the diatom is nanosized silica. Although some papers reported photoluminescence emitted from bulk amorphous silica, their measurements were accomplished under very low temperature, i.e. 90K. There is no report of the photoluminescence of bulk amorphous silica at room temperature. Fig.35 shows the emission spectra of diatom sample and bulk amorphous silica. Apparently, the bulk amorphous silica does not emit light under the same measurement condition as the diatom sample.

Comparison of emission spectra of diatom and bulk amorphous SiO_2

Legend: ------ Ni22-5-1-H2O2 ; ——— bulk amorphous SiO2
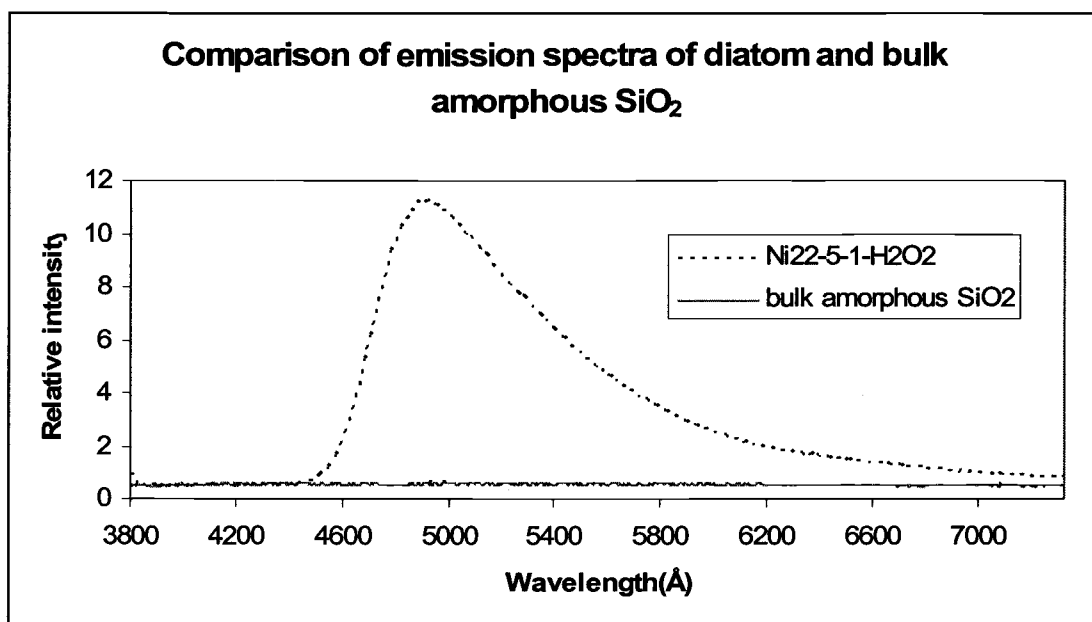
Fig.35 Comparison of emission spectra of diatom and bulk amorphous silica

4.5.6 Comparison of emission spectra of samples treated with different methods

Four different methods were used to treat the sample, and the corresponding emission spectra are shown in Fig.36.
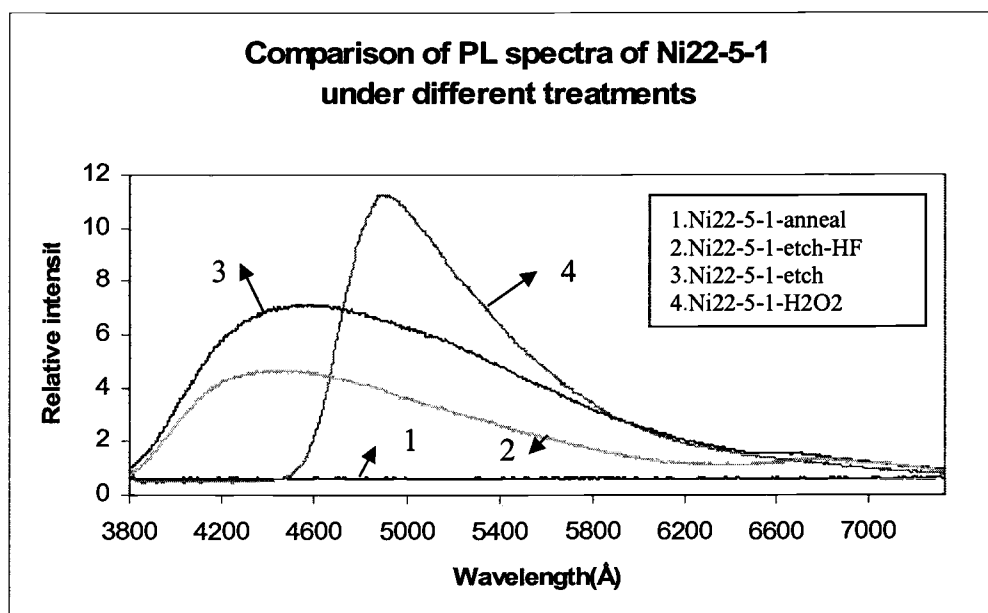
Fig.36 Emission spectra of diatom sample with different treatments

The spectra in Fig.36 show that the treatment method affects the photoluminescent property of diatom significantly. The annealed sample does not emit light; the etched sample has a broad emission peak centered at 430nm; the hydrogen fluoride treatment does not affect the photoluminescence (more studies should be considered); the sample treated with peroxide has a comparatively narrow emission peak centered at 480nm. Combining with XRD data, we can explain why the sample did not show photoluminescence when it was treated with 800°C annealing. The XRD data show SiO_2 reacted with CaO and other components when the diatom sample was annealed at

800°C, so silica was converted to silicate grain and lose nanoscale feature. It is hard to explain why the peaks of the light emitted from the same sample but treated with H_2O_2 and oxygen plasma etching are centered at different positions. It is noticed that the etched sample has a broader peak than the sample treated with H_2O_2. One possibility regarding the different appearance of PL spectra is that the PL spectrum of the etched sample is overlapped by more than one peak, including the peak centered at 480nm. This is worthy further study in the future.

4.5.7 Summary of photoluminescence experiments

Diatom samples (no matter with addition of germanium or not) treated with H_2O_2 or oxygen plasma can emit visible light at room temperature when the excitation light is at 335nm, but no photoluminescence occurs when they are treated with 800°C annealing. For samples treated with H_2O_2, those without the addition of germanium emit greenish blue light centered at 480nm, and those with the addition of germanium emit blue light centered at 430nm. On the other hand, for samples treated with oxygen plasma, no matter with or without addition of germanium, they have very similar emission spectra. All of them have a broader peak than samples treated by H_2O_2, and the peak is centered at 430nm. Very importantly, compared with the diatom samples, the bulk amorphous silica does not show any photoluminescence under the same measurement conditions.

4.5.8 Photoluminescence mechanism of diatom

The photoluminescence of diatoms has not been reported so far, so the detail discussion about the mechanism will be exploited here.

From the previous studies of diatoms, such as FT-IR and TEM-EDS, we know the major component of diatoms is nano-sized amorphous SiO_2 (silica). Consequently, the photoluminescence emitted from diatom should be closely related to the nano-sized amorphous silica. Some researchers[32] studied PL property of synthesized silica, and they observed the similar blue PL for bulk crystalline and amorphous SiO_2. They concluded that the PL is mostly associated with self-trapped excitons (STE). Some researchers pointed out that the STE PL is peaked between 2.6 and 2.8eV for crystalline SiO_2, whereas it is extended over the entire visible spectral range with a maximum between 2.2 and 2.4eV for amorphous silica. The difference of the peak positions of the STE PL reflects the features of the self-trapped exciton formation in crystalline and amorphous SiO_2. The same paper also studied the photoluminescence of silica nanoparticles, under the excitation of 6.4 eV laser light. The silica nanoparticles with dimension of 15nm exhibit three strong emission bands at ~1.9eV (red), ~2.35eV (green) and 2.85-3.25eV (blue) band. The paper suggested that the red and green PL from silica nanoparticles are due to non-bridging oxygen hole centers (NBOHC's), hydrogen-related species and STE's respectively. In that paper, the STE PL band is peaked at ~2.75eV for both bulk amorphous and crystalline SiO_2. The main difference between the PL spectra for silica nanoparticles and bulk fused silica is the blueshift of the STE PL band for nanoscale materials. Also the STE PL band is blueshifted with decreasing nanoparticle size.

Although the measurements done in that paper were under different conditions than that in this thesis (most important difference is the high excitation light at 6.4eV

in that paper), the data above from the paper provided a comparison with the results of the photoluminescence from diatoms. The differences and compatibilities between the PL experiments in the paper and that in this thesis include the following. (1) The material in the paper is pure synthesized SiO_2 nanoparticles (7nm and 15nm), but in this thesis the material is the naturally biomineralized SiO_2 nanomaterial (~30nm) which comprises some impurities. (2) Both of them have blue emission band, though the center peak position for the blue bands are a little bit different. In that paper, the blue band is at 2.85 eV for 15 nm SiO_2 and 3.25 eV for 7nm SiO_2, but it is at 2.6eV for the diatom samples. Based on the above data, we can explore and propose the mechanism of photoluminescence from diatoms.

The photoluminescence spectra from diatoms without the addition of germanium (Fig. 30) consist of one broad asymmetric peak centered at around 480nm (2.6 eV), which most likely include a peak around 2.35 eV (green) because of its asymmetry. Also the peak at 670 nm (1.85 eV) from diatoms matches the peak of 1.9 eV for the synthesized SiO_2 nanoparticles. These comparisons indicate that the photoluminescence generated from diatoms is due to non-bridging oxygen hole center (1.85 eV), hydrogen-related species (2.35 eV) and self-trapped exciton (2.6 eV) in the diatom samples. Because the most intense photoluminescence is at 2.6 eV, we propose that the major reason caused the PL from diatoms could be self-trapped excitons (STE) and quantum confinement effect.

The first concept about the mechanism of the photoluminescence from diatoms should easily come up with quantum confinement effect (QCE), because the cell wall

of diatoms is consisted of nanosized SiO_2. Quantum confinement effect is used to describe some phenomena occurred when the diameter of the particle is of the same order of magnitude as the wavelength of the electron wavefunctions. In that case, lots of properties, specially the optical and electronic properties of the material have some deviations from their bulk materials. The energy spectrum changes from continuous for bulk material to discrete for materials consisted with nanoparticles. The QCE will affect the band-band electronic energy change, as well as excitons. A common finding about QCE is the inverse correlation of the optical gap with the particle size. Based on this common observation, the bandgap of nanostructured SiO_2 in diatoms should be higher than 8.6eV which is the bandgap of SiO_2 bulk material. With this high bandgap, electrons are hard to be excited from the valence band to conduction band. In this thesis, the excitation light is 335nm (3.7eV) which is much lower than the bandgap of the diatom sample. Furthermore, with 3.7eV excitation light, the luminescence measured from the diatom samples should not be caused by band-to-band transition. Consequently even if the quantum confinement effect (QCE) affects the band-band transition in diatoms, we are not able to measure it.

It has been mentioned previously that the most possible reason for photoluminescence from diatoms is caused by self-trapped exciton under quantum confinement effect. The optical excitation of materials results in a sudden change of electronic charge distribution, thereby destroying the balance of interatomic forces, generating potential well, and forming exited electrons and valence hole. The bound of a pair of electron and hole is referred to as the free exciton (FE). The electrons and

holes can cause large distortions in the structure surrounding them. If the distortion

energy is high, electrons and holes are made immovable and are self-trapped, because

the self-trapped state is more stable than the one in which they would move dragging

the distortions. By definition, self-trapped exciton (STE) means that the exciton

becomes stabilized by localizing themselves in the potential well due to the self-

induced lattice distortion. Oxygen-distorted STE is a common STE in SiO_2 structure

and its formation is illustrated in follows based on the calculation of semiempirical

(INDO) approach[33]. The entire process of STE formation because of oxygen-distortion

is discussed here. The self-trapped exciton model of SiO_2 is illustrated in Fig.37.

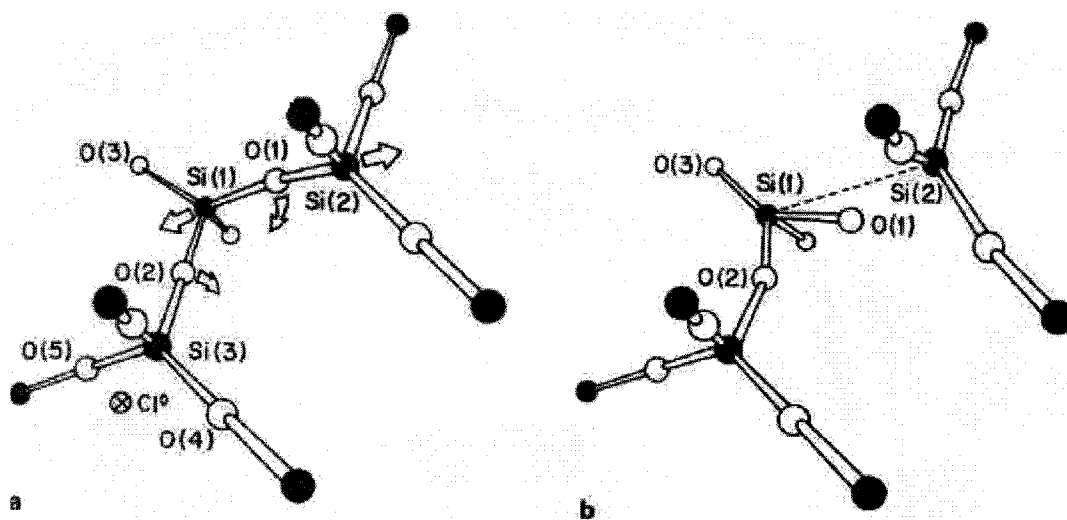Fig.37 Self-trapped exciton model of SiO_2 (cited from reference 33)

The oxygen atom labeled O(1) is moved perpendicular to the Si-O-Si linear bond

axis in the arrow direction. As the energy minimization proceeds, the atomic

relaxation occurs. This displacement of O(1) is sufficient to cause 70% localization of

the hole spin density on that oxygen atom and about 45% electron localization on the

adjacent silicon atoms Si(1) and Si(2). As the relaxation of O(1), O(2), Si(1) and Si(2) is allowed to proceed to the minimum energy configuration. Finally, the hole is almost completely localized on O(1), the Si(2)-O(1) bond is weakened as a missing bond. Researchers simulated this process and found that the hole component of the exciton in this model is almost completely localized onto a specific oxygen. The electron distributes more diffusely, centered at the oxygen vacancy.

It is worth mentioned that most photoluminescence should be measured at low temperature, because luminescence efficiency is higher at low temperature (such as 90k) than that at high temperature. At high temperature, the thermal energy of excitons will be increased and the binding energy between electrons and holes will be decreased, so the electron and hole pair composing an exciton will be easily departed. Furthermore the possibility of luminescence caused by excitons will be dramatically declined, because the chance of recombination of the electron and hole is significantly reduced. However, under the quantum confinement effect, the excitons are confined and trapped within a certain field without departure even at high temperature. This is why the strong blue photoluminescence was observed from diatom samples even at room temperature.

Generally speaking, impurity can affect the luminescence. The appearance of foreign atoms leads to local disturbances in the periodicity of the potential field. At small concentrations of impurities the electrons and holes are bound to one another and cannot move. At high concentration of impurities, the wavefunctions of electrons belonging to different atoms overlap, so the impurity bands merge with the parent

bands. This will definitely affect the luminescence property of the parent material. By comparing the influence of HF treatment on photoluminescence shown on Fig.36, it is observed that HF treatment do not affect the photoluminescence much. In fact, there are two purposes of treating the etched sample with HF. One is to study how the impurity affects the PL property, because some impurities are supposed to be gotten rid of the material after HF treatment. Another purpose is to observe if the pore size of the cell wall can affect the PL property. From the result shown in Fig.36 we can roughly conclude that neither impurity nor pore size affects the PL property of diatom. (Here we assume the pore size of the cell wall is enlarged after 20minutes HF treatment.)

Based on the analysis above, we conclude that the photoluminescence from diatom is mainly caused by self-trapped exciton (STE) combining quantum confinement effect (QCE).

Conclusion

Several techniques, such as ICP, FT-IR, XRD, SEM/EDS and TEM/EDS were useed to characterize the diatom samples cultivated in bioreactors. Combining all the results obtained from the techniques above, a comparatively complete characterization of diatom species, *Nitzschia frustulum,* was figured out. One very important property of diatom, photoluminescence was characterized.

ICP technique is a reliable tool to identify the element constituents of the sample. It showed that the average weight ratio of Ca/Si is about 1:3. It can be used to accurately track the amount of Ge uptaken by the diatom sample, so that the mechanism of the element uptake would be clarified. The sample for accurate ICP analysis should be the original green cell mass without any treatments like annealing and oxygen plasma etch.

FT-IR is an easy way to analyze the bonding information of compounds. The distinguishable differences between samples could be observed. Some samples added with germanium were observed containing GeO_2. The diatom samples without addition of germanium mainly consists of amorphous calcium carbonate, calcite (crystal $CaCO_3$) and $[SiO_4]^{4-}$ network. The sample should be treated with thermal annealing or oxygen plasma, in order to get rid of the interference of the organic materials.

XRD provided an indirect perspective to carry out the components of diatom. This is an efficient and a complementary technique to understand the structures of the components. Annealing treatment should be conducted to assure that crystal structure

is formed, in order to observe the signals. The XRD result also showed GeO_2 should be formed inside the diatom cells.

SEM/EDS and TEM/EDS are the advanced techniques to inspect diatom shell shape, surface topology, to identify the location of a certain element and to provide a quantitative analysis for the element composition of diatom material. Germanium was found for some samples and the preliminary result showed that the germanium is located on the inside edge of the diatom cell.

Photoluminescent property of diatom was studied. The strong greenish blue photoluminescence centered at 480nm was observed for diatom samples without the addition of germanium, and the strong blue photoluminescence centered at 430nm was detected for samples with the addition of germanium. Besides, the sample treatments effect the photoluminescence, for example, samples treated with thermal annealing did not show any visible photoluminescence, and samples treated with H_2O_2 show more narrow photoluminescence peak than the samples treated with oxygen plasma.

Future Works

There are three very important works need further study.

First of all, the location of germanium needs a more accurate description, so the ultra-sectioning and TEM observation should be done to accomplish this purpose.

Secondly, the photoluminescent property for the bulk material has been done in this thesis, but weather the pore size of the diatom shell affects the PL property or not and how it affects the PL property needs further investigation.

Thirdly, proper application of diatom based on its photoluminescence property would be a very interesting topic.

Reference Cited

1. S. Mann and G.A. Ozin. Synthesis of inorganic materials with complex form. *Nature*, 382, 313-318 (1996).

2. C.R. Lowe. Nanobiotechnology: the fabrication and applications of chemical and biological nanostructures. *Current Opinion in Structural Biology*, 10, 428-434 (2000).

3. N. Kröger, R. Duetzmann, and M. Sumper. Polycationic peptides from diatom biosilica that direct silica nanosphere formation. *Science*, 286, 1129-1132 (1999).

4. K. Rajeshwar, N.R de Tacconi, and C.R. Chenthamarakshan. Semiconductor-based composite materials: preparation, properties, and performance. *Chem. Mater.* 13, 2765-2782 (2001).

5. Clayton S. Jeffryes, Oregon State University M. S. thesis, 2005.

6. Richard P. Feynman. There's plenty of room at the bottom. *Caltech's Enginnering Science*, February, 22-36 (1960).

7. Interagency Working Group on Nanoscience, Engineering and Technology, National Nanotechnology Initiative Leading to the Next Industrial Revolution, February (2000).

8. http://www.foresight.org/NanoRev/

9. Alfred E. Brenner. Moore's law. *Science*, 275, 1401-1404 (1997).

10. R. W. Drum and R. Gordon, Star Trek replicators and diatom nanotechnology, *TibTech (Trends in Biotechnology)*, 21, 325 (2003).

11. F. E. Round, R. M. Crawford, and D. G. Mann, *The diatoms: Biology and morphology of the genera*, Cambridge University Press, New York(1990).

12. P. Cohen, Natural glass. Why bother laboriously creating intricate, microscopic devices when single-celled organisms can do the job for you? Philip Cohen meets nanotechnology's master craftsmen, *New Scientist*, 181, 26 (2004).

13. V. Martin-Jézéquel, M. Hildebrand, and M.A. Brzezinaski, Silicon metabolism in diatoms: implications for growth. J. Phycol. 36, 821-840 (2000).

14. M. Hildebrand. Silicic acid transport and its control during cell wall silicification in diatoms, in *Biomineralization: from Biotechnology to Medical Application*, edited E. Baeuerlein, Wiley-VCH, Weinheim (2000), pp. 171-188.

15. J. Pickett-Heaps, A. Schmid, and L.A. Edgar. The cell biology of diatom valve formation, in *Progress in Phycological Research*, edited F.E. Round and D.J. Chapman, Biopress Ltd, Bristol (1990), pp. 1-168.

16. N. Kröger, S. Lorenz, E. Brunner, and M. Sumper. Self-assembly of highly phosphorylated silaffins and their function in biosilica morphogensis. *Science,* 298, 584-586 (2002).

17. M. Sumper. A phase separation model for the nanopatterning of diatom biosilica. *Science,* 295, 2430-2433 (2002).

18. B.E. Volcani. Cell wall formation in diatoms: morphogenesis and biochemistry, in *Silicon and Siliceous Structures in Biological Systems*, edited T.L. Simpson and B.E. Volcani (1981), pp. 57-200.

19. F. Noll, M. Sumper, and N. Hampp. Nanostructure of diatom silica surfaces and of biomimetic analogues. *Nano Letters*, 2, 91-95 (2002).

20. S. Crawford, M.J. Higgins, P. Mulvaney and R. Wetherbee. Nanostructure of the diatom frustule as revealed by atomic force and scanning electron spectroscopy. *J. Phycol.* 37, 543-554 (2001).

21. K. H. Sandhage, M. B. Dickerson, P. M. Huseman, Reactive Conversion of Diatom Frustules: A Novel, Hybrid Route to Complex-Shaped Microstructures with Tailored Chemistries, *Advanced Materials,* 14, 429(2002).

22. F. Azam, B.B. Hemmingsen, and B.E. Volcani. Germanium incorporation into the silica of diatom cell walls. *Arch. Mikrobiol,* 92, 11-20 (1973).

23. F. Azam and B.E. Volcani. Role of silicon in diatom metabolism. VI. Active transport of germanic acid in the heterotrophic diatom *Nitzschia alba*. *Arch. Mikrobiol,* 101, 1-8. (1974).

24. M.L. Chaippino, F. Azam, and B.E. Volcani. Effect of germanic acid on developing cell walls of diatoms. *Protoplasma*, 93, 191-204 (1977).

25. http://www.inchem.org/documents/ehc/ehc/ehc24.htm (3/11/2005).

26. E. Beniash, J. Aizenberg, L. Addadi, S. Weiner, Amorphous calcium carbonate transforms into calcite during sea urchin larval spicule growth, *Proc. R. Soc. Lond. B*, 264, 461-465(1997).

27. S. Raz, O. Testeniere, Stable amorphous calcium carbonate is the main component of the calcium storage structures of the crustacean *orchestia cavimana, Biol. Bull,* 203, 269-274(2002).

28. R. J. Kingsley, R. V. Gilder, Multimineral calcareous deposits in the marine alga *ACETABULARIA ACETABULUM, J. Phycol.,* 39, 937-947(2003).

29. J. H. Park, D. J. Min and H. S. Song, FT-IR spectroscopic study on structure of CaO-SiO2 and CaO-SiO2-CaF2 slags, *ISIJ International*, 42, 344-351(2002).

30. A.Margaryan and M. A. Piliavin, *Germanate Glasses*, Artech House, InC.1993, Chap. 3, pp.28.

31. G. L. Rorrer, C-H Chang, S-H Liu, C. Jeffryes, Biosynthesis of Silicon-Germanium Oxide Nanocomposites by the Marine Diatom Nitzschia frustulum, *Journal of Nanoscience and Nanotechnology,* 5, 41-49(2005).

32. Y. D. Glinka, Time-resolved photoluminescence study of silica nanoparticles as compared to bulk type-III fused silica, *Physical Review B,* 66, (2002).

33. A. K. S. Song, R.T. Williams, Self-trapped exciton, pp276(1993).